The Absolute Magnitude and Kinematics of RR Lyrae Stars via Statistical Parallax

Andrew C. Layden
Department of Physics & Astronomy,
McMaster University, Hamilton, Ontario, L8S 4M1, Canada
layden@physics.mcmaster.ca

Robert B. Hanson
University of California Observatories / Lick Observatory,
University of California, Santa Cruz, CA 95064
hanson@ucolick.org

Suzanne L. Hawley[1]
Department of Physics & Astronomy, Michigan State University, E. Lansing, MI 48824
slh@pillan.pa.msu.edu

Arnold R. Klemola
University of California Observatories / Lick Observatory,
University of California, Santa Cruz, CA 95064
klemola@ucolick.org

Christopher J. Hanley
Department of Physics & Astronomy, Michigan State University, E. Lansing, MI 48824
chris@pillan.pa.msu.edu

ABSTRACT

We present new statistical parallax solutions for the absolute magnitude and kinematics of RR Lyrae stars. We have combined new proper motions from the Lick Northern Proper Motion program with new radial velocity and abundance measures to produce a data set that is 50% larger, and of higher quality, than the data sets employed by previous analyses. Based on an *a priori* kinematic study, we separated the stars into halo and thick disk sub-populations. We performed statistical parallax solutions on these sub-samples, and found $M_V(RR) = +0.71 \pm 0.12$ at $\langle[\mathrm{Fe/H}]\rangle = -1.61$ for the halo (162 stars), and $M_V(RR) = +0.79 \pm 0.30$ at $\langle[\mathrm{Fe/H}]\rangle = -0.76$ for the thick disk (51 stars). The solutions yielded a solar motion $\langle V\rangle = -210 \pm 12$ km s^{-1} and velocity ellipsoid $(\sigma_U, \sigma_V, \sigma_W) = (168 \pm 13, 102 \pm 8, 97 \pm 7)$ km s^{-1} for the halo. The values were $\langle V\rangle = -48 \pm 9$ km s^{-1} and $(\sigma_U, \sigma_V, \sigma_W) = (56 \pm 8, 51 \pm 8, 31 \pm 5)$ km s^{-1} for

[1]NSF Young Investigator

the thick disk. Both are in good agreement with estimates of the halo and thick disk kinematics derived from both RR Lyrae stars and other stellar tracers. Monte Carlo simulations indicated that the solutions are accurate, and that the errors may be smaller than the estimates above. The simulations revealed a small bias in the disk solutions, and appropriate corrections were derived. The large uncertainty in the disk $M_V(RR)$ prevents ascertaining the slope of the $M_V(RR)$–[Fe/H] relation. Using a zero point defined by our halo solution and adopting a slope of 0.15 mag dex^{-1}, we find that (1) the distance to the Galactic Center is 7.6 ± 0.4 kpc; (2) the mean age of the 17 oldest Galactic globular clusters is $16.5^{+2.1}_{-1.9}$ Gyr; and (3) the distance modulus of the LMC is 18.28 ± 0.13 mag. Estimates of H_0 which are based on an LMC distance modulus of 18.50 (e.g., Cepheid studies) increase by 10% if they are recalibrated to match our LMC distance modulus.

1. Introduction

The absolute magnitude of the RR Lyrae variables, $M_V(RR)$, is integral to determining distances to old stellar systems in our Galaxy and to other nearby galaxies. For example, RR Lyraes are widely used to measure the distances to Galactic globular clusters, to the Galactic Center, and to many members of the Local Group. In addition, the distances to individual field RR Lyrae stars in the thick disk and halo of our Galaxy enable us to determine the kinematic and spatial distributions of these populations.

Precise distances to globular clusters are also necessary to determine their ages (e.g., Buonanno *et al.* 1989). The variation of $M_V(RR)$ with abundance, [Fe/H], strongly affects the derived age spread and age-metallicity relation of the Galactic globular cluster system. These quantities in turn place strong constraints on scenarios describing the formation of the Galaxy, specifying the rate of halo formation and whether the chemical enrichment of the halo proceeded in a uniform, global fashion, (Eggen *et al.* 1962) or within autonomous star-forming fragments (Searle & Zinn 1978). The zero-point of the $M_V(RR)$–[Fe/H] relation sets the mean absolute age of the globular cluster system, thus placing a critical lower limit on the age of the Universe.

The RR Lyraes in a given globular cluster are observed to have a very narrow range of intensity-mean magnitudes, typically $\sigma_V = 0.06$–0.15 mag (Sandage 1990a). Though the $M_V(RR)$ variation from cluster to cluster over a broad range in [Fe/H] is not so well understood, it is clear that RR Lyrae stars have the potential to be excellent standard candles.

Historically, there has been discussion over the slope of the $M_V(RR)$–[Fe/H] relation, with values ranging between $\Delta M_V/\Delta$[Fe/H] = 0 to 0.4 mag dex^{-1} (corresponding to a globular cluster age range of $\gtrsim$5 Gyr to approximately zero). Recently, a consensus has begun to form that the slope has a value of 0.15–0.20 (e.g., Carney *et al.* 1992 and Chaboyer 1995, though see Sandage 1993 and Mazzitelli *et al.* 1995 for dissenting opinions).

However, the zero-point of the relationship continues to defy a consensus. At the characteristic abundance of the halo, [Fe/H] = –1.6, $M_V(RR)$ values range from 0.45 to 0.75 mag, and usually fall either toward the brighter or the fainter end of this range. Chaboyer (1995) showed that this "two value" effect translates to a $\sim$22% difference in the derived ages of the Galactic globular clusters, and in fact represents the dominant uncertainty in the determination of cluster ages.

A number of methods have been used to estimate $M_V(RR)$, including Baade-Wesselink (surface brightness) analyses (Jones *et al.* 1992), main sequence fitting of globular clusters (Buonanno *et al.* 1989), application of stellar pulsation theory to field stars (Sandage 1990b), horizontal branch evolution theory (Lee *et al.* 1990), calibrating the LMC RR Lyraes using other LMC distance estimates (Walker 1992, Gould 1995), and the statistical parallax method (Hawley *et al.* 1986, Strugnell *et al.* 1986).

The essence of the statistical parallax ("stat-π") method is to balance the radial-velocity-derived kinematics of a homogeneous stellar sample with its kinematics as derived from proper motions. The former are independent of distance, while the latter are distance-dependent. They are balanced through a simultaneous solution for a distance scale factor. Hawley *et al.* (1986) discussed the stat-π solutions performed prior to 1985, and described the shortcomings in the methods that were employed. They argued that only a complete treatment using a maximum-likelihood formulation, together with a minimization technique which is tolerant of inter-dependent variables, can produce accurate solutions.

Two modern studies have employed these techniques (Hawley *et al.* 1986, and Strugnell *et al.* 1986, hereafter referred to as HJBW and SRM, respectively). HJBW compiled proper motion, radial velocity, apparent magnitude, and abundance data from the literature to produce a sample of $\sim$140 stars. SRM employed the virtually same set of data. The two groups obtained similar values for $M_V(RR)$, the only difference being in the details of the adopted reddenings and determination of the apparent magnitudes. Both groups concluded that the sample was too small to constrain the slope of the $M_V(RR)$–[Fe/H] relation.

Since then, considerable new data have become available, indicating that it is an opportune time for a new stat-π analysis. The Lick Northern Proper Motion (NPM) program (Klemola, Jones & Hanson 1987) has measured absolute proper motions for over 1000 RR Lyrae stars. These data are more uniform and have a more accurate zero-point than the proper motions employed in previous analyses, mainly because the plates, obtained from a single telescope and covering most of the Northern hemisphere, were measured and reduced onto a single inertial frame tied to external galaxies. Meanwhile, Layden (1994) determined abundances and radial velocities for over 300 RR Lyraes, including most of those in the HJBW and SRM studies. Blanco (1992) showed that the abundances used in those studies were of variable accuracy and zero-point. Layden's [Fe/H] measures are on a self-consistent system and are typically accurate to 0.15–0.20 dex. Thus, a new stat-π solution will reap the benefits of a 50% larger sample size (213 stars) and higher quality data.

Furthermore, Layden (1995) showed that the local RR Lyrae sample breaks fairly cleanly into thick disk and halo populations at [Fe/H] = –1. The existence of two kinematically distinct populations had not been recognized in previous stat-π studies, in part because the existing ΔS abundances were of insufficient accuracy to provide the the required abundance resolution. As a result, the two populations had been mixed. One worries that such mixing might have resulted in the $M_V(RR)$–[Fe/H] slope being under-estimated. In the worst case, population mixing might lead to errant solutions, since the stat-π method is a simultaneous solution for kinematics and $M_V(RR)$. We consider it safest to treat the disk and halo separately in our solutions.

This paper reports the findings of our new stat-π solutions, based on the improvements described above. Throughout the paper, we employ the stat-π code used by HJBW. In Sec. 2, we describe in detail the data used in our stat-π solutions. In Sec. 3, we begin our analysis with an inverted approach; we assume an $M_V(RR)$–[Fe/H] relation, and compute the distance and three space velocity components of each RR Lyrae star in our sample. This gives us insight into how best to divide the sample during the stat-π solutions. In Sec. 4, we present Monte Carlo simulations which enable us to investigate the accuracy of our solutions, and to search for any inherent biases produced by the stat-π technique. In Sec. 5, we present the absolute magnitude and kinematic results of the stat-π solutions for the observed stars. In Sec. 6, we compare our $M_V(RR)$ results with those obtained by other authors using other techniques. In Sec. 7, we discuss the implications of our results for some basic properties of the Galaxy and the Universe. We close with a short summary of our findings.

2. Data

2.1. Proper Motions

Our primary source of proper motions for this study is the Lick Northern Proper Motion (NPM) program (Klemola, Jones & Hanson 1987). The NPM program is a photographic survey measuring precise absolute proper motions, on an inertial system defined by 50,000 faint galaxies ($16 \lesssim B \lesssim 18$), for over 300,000 stars with $8 \lesssim B \lesssim 18$, covering the northern two-thirds of the sky ($\delta > -23°$), based on plates taken between 1947 and 1988 with the Lick 51 cm Carnegie Double Astrograph. Details of the NPM observing, plate measurement, and reduction procedures are given by Klemola *et al.* (1987).

Part I of the NPM program, covering the 72% of the northern sky lying outside the heavily obscured regions of the Milky Way, was completed in 1993, with the release of the Lick NPM1 Catalog (Klemola, Hanson & Jones 1993; Hanson 1993), containing 149,000 stars. The stellar content of the NPM1 Catalog is detailed in the NPM1 Cross-Identifications (Klemola, Hanson & Jones 1994a; Hanson & Klemola 1994). Comprehensive error analyses (Klemola, Hanson & Jones 1994b) have determined the RMS error of the NPM absolute proper motions to be $\sigma_\mu = 0\farcs5$ cent^{-1} in each coordinate, corresponding to a transverse velocity error ~ 25 km sec^{-1} kpc^{-1}. The NPM1

Catalog contains over 1000 RR Lyrae variables (Klemola *et al.* 1994a, Appendix 2). Some 300 of these have $B < 14$ (corresponding to $D \lesssim 4$ kpc) and may be individually useful for stat-π studies.

The particular value of the NPM proper motions for this work is that they are on an absolute reference frame. By contrast, previous RR Lyrae stat-π solutions have relied on relative proper motions, measured with respect to field stars (generally with $10 \lesssim B \lesssim 12$), and corrected to absolute by assuming the net motions of the reference stars from models of Galactic kinematics and rotation. Using relative proper motions inevitably raises the possibility that the resulting kinematics (and luminosities) may depend to some extent on the input assumptions.

Specifically, the HJBW and SRM stat-π solutions used the list of proper motions for 168 RR Lyraes compiled by Wan, Mao & Ji (1980; hereafter referred to as WMJ). WMJ added new relative proper motions from the Shanghai Observatory (Wan, He, Zhu & Li 1979) and other sources to the previous such compilation by Hemenway (1975).

Because of their absolute character, we adopted the NPM proper motions as the primary source for our stat-π database. Our search of the NPM1 Catalog, using the NPM1 Cross-Identifications, found 171 RR Lyrae stars from Layden's (1994) list. However, the NPM1 Catalog does not cover low Galactic latitudes ($|b| \lesssim 10°$), nor the southern sky below $-23°$ declination. To attain the complete sky coverage needed for reliable stat-π solutions, we used the WMJ compilation as a secondary source where NPM proper motions were not available, adding another 42 stars. Using the WMJ data raises two practical problems:

First, should the WMJ motions be corrected to the NPM absolute system? The heterogeneous nature of the WMJ compilation might make any single correction doubtful. However, Clube & Dawe (1980b) suggested that the existing RR Lyrae proper motions needed a large correction "in the direction of Galactic rotation" $\Delta\mu = -1\farcs4 \pm 0\farcs8$ cent^{-1} due to incorrect motions of the reference stars, making $M_V(RR)$ ~ 0.05 to 0.1 mag fainter. So large a systematic error should be easily detectable by comparing the NPM and WMJ proper motions.

Second, how should the WMJ data be weighted relative to the NPM motions? WMJ estimated the errors for each star from the repeatability of the existing proper motions for that star, but the number of determinations is generally small, so these estimates may not be individually reliable. For example, the range of σ_μ(WMJ) is very large, some values are incredibly small (one is zero!), and the correlation between each star's right ascension and declination proper motion errors is very poor. One-fourth of the WMJ stars have σ_μ in one coordinate more than three times the value in the other coordinate. Because all the sources cited in WMJ used methods which should produce errors of equal size in either coordinate, this is plainly an artifact of the WMJ error analysis. However, the overall mean and RMS errors ($0\farcs49$ and $0\farcs68$ cent^{-1} in μ_α; $0\farcs43$ and $0\farcs61$ cent^{-1} in μ_δ) are quite comparable to values given in the literature (Wan *et al.* 1979; Hemenway 1975), and may in fact be reliable error estimates.

To answer these questions, we compared data for the 109 stars in common between the NPM1 Catalog and the WMJ compilation. The comparison was done twice; using $\Delta\mu = \mu(\text{NPM}) -$

μ(WMJ) in equatorial coordinates (α, δ) and in Galactic coordinates (l, b). Normal probability plots (Lutz & Hanson 1992) were used for robust estimates of the mean differences and RMS dispersions. Plots of $\Delta\mu$ vs. μ, α, δ, l, b and magnitude were examined for any dependence on these observational variables. Finally, we assessed the significance of the WMJ individual proper motion errors σ_μ(WMJ). Two principal results were found, bearing on each of the questions posed above.

First, the WMJ proper motions in Galactic longitude have a small but significant mean difference with NPM1. We found

$$< \Delta\mu_l > = \; -0\overset{\prime\prime}{.}23 \pm 0\overset{\prime\prime}{.}08 \text{ cent}^{-1}$$

$$< \Delta\mu_b > = \; -0\overset{\prime\prime}{.}03 \pm 0\overset{\prime\prime}{.}08 \text{ cent}^{-1}.$$

As Clube & Dawe (1980b) suggest, such a systematic difference may reflect erroneous reference star motions, but our result is six times smaller than theirs. Consequently, any effects on $M_V(RR)$ would be at the 0.01 mag level. So, there is no need to correct the WMJ data for our stat-π solutions.

Second, the WMJ proper motion errors are only useful as an overall average, not on a star-by-star basis. Figure 1 shows the NPM–WMJ proper motion differences versus the WMJ listed errors. In each coordinate, the stars with the smaller errors ($\sigma_\mu \sim 0\overset{\prime\prime}{.}2$ cent^{-1}) scatter just as much as the stars with the larger errors ($\sigma_\mu > 0\overset{\prime\prime}{.}4$ cent^{-1}). For the very smallest errors ($\sigma_\mu < 0\overset{\prime\prime}{.}1$ cent^{-1}) the scatter is smaller, but the offsets from zero are large. A constant error describes the data much better than does the large variation in σ_μ(WMJ).

Figure 2 quantifies this, testing whether the RMS error actually increases with σ_μ. In each coordinate, the 109 stars were sorted by the size of σ_μ(WMJ). Figure 2 plots the running values of the RMS nominal error and the actual RMS dispersion of $\Delta\mu$ as a function of this rank. The nominal error σ(TOT) is the quadratic sum of σ_μ(WMJ) and $0\overset{\prime\prime}{.}5$ cent^{-1} $= \sigma_\mu$(NPM). The smooth, slowly rising curve labeled "tot" in Figure 2 is the running RMS value of σ(TOT). If the WMJ errors are correct, then $\sigma(\Delta\mu)$, the RMS dispersion of the proper motion differences, should follow this curve. The jagged line labeled "$\Delta\mu$" traces the running value of the actual RMS dispersion. In each coordinate, $\sigma(\Delta\mu)$ quickly rises to a large value ($\sim 0\overset{\prime\prime}{.}85$ cent^{-1} in μ_α, $\sim 0\overset{\prime\prime}{.}80$ cent^{-1} in μ_δ) by rank ~ 10, and remains at that level out to rank $\gtrsim 100$, rising somewhat at the end. This proves that the real error of the WMJ proper motions is roughly constant, independent of the listed error σ_μ(WMJ). Quadratically subtracting σ_μ(NPM) $= 0\overset{\prime\prime}{.}5$ cent^{-1} from these values gives σ_μ(WMJ) $= (0\overset{\prime\prime}{.}69,\ 0\overset{\prime\prime}{.}62)$ cent^{-1} in (α, δ). Almost identical error estimates were obtained from normal probability plots of $\Delta\mu(\alpha, \delta)$. These estimates agree almost perfectly with the RMS values of the WMJ errors cited above.

In view of this result, we gave all WMJ proper motions equal weights in our stat-π solutions. Test solutions with σ_μ(WMJ) $= 0\overset{\prime\prime}{.}5$ and $0\overset{\prime\prime}{.}7$ cent^{-1}, corresponding to the mean and RMS WMJ errors, respectively, gave very similar results. We decided to adopt the smaller value, σ_μ(WMJ) $=$

$0''\!.5$ cent^{-1} = σ_μ(NPM), in order to weight all areas of the sky equally in the stat-π solutions (Section 5).

2.2. Abundances

Our primary source for RR Lyrae metal abundances is the work of Layden (1994, hereafter referred to as L94). These abundances are based on the relative strengths of the Ca II K line and the Balmer lines Hδ through Hβ, analogous to the ΔS abundance technique of Preston (1959). The abundance scale is tied to the [Fe/H] abundance scale for globular clusters developed by Zinn & West (1984), and the individual [Fe/H] values are typically accurate to 0.15–0.20 dex. Lambert *et al.* (1995) have measured new high-dispersion abundances for a number of the stars in L94, and find excellent agreement with those results. Jurcsik & Kovacs (1996) also discuss the high quality of the L94 abundances.

Previous statistical parallax solutions have used ΔS values as the metallicity indicator. Since then, Blanco (1992) has shown that ΔS values available to those authors were of variable accuracy and zero-point. The [Fe/H] sample of L94 is both self-consistent and contains many more stars than a sample of ΔS values collected from the literature.

However, there are a few bright RR Lyraes in the literature which are not included in the list of L94. For these, we adopt the literature ΔS values, converted to [Fe/H] using Eqn. 6 of L94. We note that some of these values, those taken from Hemenway (1975), are actually *inferred* from photoelectric indices or a period-amplitude-ΔS relation. We discuss these stars further in Sec. 2.6.

2.3. Radial Velocities

L94 also measured radial velocities for the stars in his sample, and combined them with literature velocities to produce a catalog of radial velocities, the most accurate currently available, for over 300 nearby RR Lyrae stars. L94 is our primary source of radial velocities. Velocities for a few stars not observed by L94 were taken from the literature compilation shown in Table 1 of L94. We include these, adopting for their errors the typical errors for each source derived in Sec. 2 of L94.

2.4. Apparent Magnitudes

The existing photometry on field RR Lyrae stars is a surprisingly heterogeneous data set. There are three principal works in the Johnson V-band. The work of Sturch (1966) is comprised mainly of observations at minimum light; that of Bookmyer *et al.* (1977), which contains as a subset the better-known work of Fitch, Wisniewski & Johnson (1966), and is purported to be on the same photometric system; and that of Clube & Dawe (1980b, hereafter referred to as CD80).

Barnes & Hawley (1986, hereafter referred to as BH86) show that the photometric system of Sturch is in good agreement with that of CD80, and that both are offset from the work of Fitch *et al.*. We therefore adopt the CD80 photometry as the standard to which we will compare other photometric works.

Many of the existing RR Lyrae light curves have incomplete phase coverage, so it is difficult to obtain their intensity-mean apparent magnitudes with accuracy. However, various relations exist in the literature which allow this quantity to be calculated from light curve extrema, rise times, etc. (e.g., Fitch *et al.* 1966, CD80). BH86 recomputed the coefficients for two of these methods using modern, self-consistent data, and find that the method of CD80 gives the tighter relation. We adopt this parameterization along with their coefficients,

$$\langle V\rangle_I = V_{min} - 0.375\ \Delta V - 0.040,$$

where $\langle V\rangle_I$ is the intensity-mean magnitude, V_{min} is the magnitude at minimum light, and ΔV is the light curve amplitude. By using the CD80 photometry as the basis of our photometric system, and by employing intensity-mean magnitudes computed from the preceding equation, our photometry system is equivalent to that of BH86.

We computed $\langle V\rangle_I$ for the CD80 and Bookmyer *et al.* data sets, and performed a linear regression between them to obtain a transformation between the two photometric data sets (see Table 1, line 1). We then adopted data values of CD80 (57 stars) as the primary data, and supplemented it with the values from Bookmyer *et al.* that had been transformed onto the CD80 system (81 additional stars).

The resulting data set was used to transform the Walraven photometry of Lub (1977) onto the CD80 system. The transformation, given in line 2 of Table 1, is in close agreement with the relation of Pel (1976). This resulted in 7 additional stars being added to the data set.

This data set was then used to transform the CCD photometry of Schmidt *et al* (1991, 1995) onto the CD80 system (see line 3 of Table 1), adding 36 stars to the database.

Preliminary photometry from Layden (1996; 8 stars) was also included, though no transformations were possible since there were no stars in common with the database. Data for 24 additional stars were adopted from the photometric compilation of L94 (his Table 9), after converting from the $\langle V\rangle_I$ definition of Fitch *et al.* 1966 to that of CD80.

Clearly, this approach is not ideal, since it relies on the statistical transformations between photometric systems, and assumes that the CD80 system is equivalent to the modern systems used by observers (e.g., Landolt 1992) and theorists (e.g., Lee *et al.* 1990). The approach has the advantage of reducing systematic errors by placing all the stars on the same photometric system. Ultimately, the transformations result in changes, typically –0.07 mag, which are small compared to the 0.2–0.3 mag disagreements which arise between different methods of measuring $M_V(RR)$. Furthermore, the sense of the transformation is to brighten the literature values; had we used the fainter photometry, the $M_V(RR)$ values we derived would have been fainter as well. Obtaining

self-consistent photometry at the level of several hundredths of a magnitude is a problem shared, but seldom mentioned, by all observers attempting to measure $M_V(RR)$.

2.5. Interstellar Absorption

SRM argued that reddenings derived from the Burstein & Heiles (1982) H I reddening maps provide the most accurate and consistent estimates of RR Lyrae reddenings, and hence absorption (we assume $A_V/E(B-V) = 3.1$). We therefore use Burstein & Heiles values when they are available, i.e., for stars more than 10° from the Galactic plane. We reduce their tabulated reddenings by an amount consistent with a uniform dust distribution with an exponential scale height of 100 pc (see L94). In most cases this is a small or negligible correction.

For stars less than 10° from the plane, we adopt the reddening values given by Blanco (1992), which are derived from the stars' colors at minimum light. When neither are available, we interpolate between the Burstein & Heiles reddening at ±10°, and that of FitzGerald (1968, 1987) at ±0.5°, at the longitude of the star. The latter is clearly a poor solution, but it is the best available until accurate minimum-light colors can be obtained for these stars. Fortunately, it was used for only 9 stars.

2.6. The Final Database

Using the data sources described above, we find that 213 stars have values for all five of the fundamental data types: proper motion, abundance, radial velocity, apparent magnitude, and reddening. This is substantially more than were used in the recent studies of HJBW (142 stars) and SRM (139 stars). Note that we do not consider Bailey type-*c* RR Lyraes in this study, only type-*ab* stars.

This database is presented in Table 2. The first column gives the variable star name, and the second column gives the NPM1 catalog number. Following this are the galactic longitude and latitude (in degrees) and the adopted proper motions in right ascension and declination (in arcsec cen^{-1}). The seventh and eighth columns give the adopted radial velocity and its error (in km s^{-1}). Next is the adopted abundance, [Fe/H]. The tenth column gives the adopted intensity-mean apparent V magnitude, and the eleventh column gives the adopted interstellar absorption. The twelfth column gives references for the sources of the proper motion, abundance, photometry, and interstellar absorption, as listed at the end of the table. The final column indicates whether a star was treated as a disk (1) or halo (0) star under the three disk/halo definitions discussed in Sec. 3.

NPM proper motions are used for 171 of the 213 stars in our sample. Abundances from L94 are used for 187 of the stars, and apparent magnitudes computed directly from V–band photometry

are used for 182 of the stars.

Given the dominance of NPM proper motions in our catalog, one wonders if the distribution of stars on the sky is skewed, and whether this would introduce a bias into our stat-π solutions (e.g., Croswell, Latham & Carney 1987). Regarding the former, we find that 63% of our sample lies above the celestial equator; we are weighted to the North celestial hemisphere, but not overwhelmingly so. Similarly, 67% of our stars lie North of the Galactic plane. However, these asymmetries can not produce the kind of biases discussed by Croswell *et al.*, since our sample contains no proper motion bias. As Klemola *et al.* (1987) describe, samples of "astrophysically interesting" stars, such as RR Lyraes, were selected for the NPM program in advance of the plate measurements, and no star was omitted from the NPM1 Catalog because its measured proper motion proved to be small. This type of pre-selection is true of our secondary proper motion source as well. As confirmation, we note that our data show no sign of the "Croswell effect." The number of stars moving away from the Galactic plane is almost identical to the number moving toward it: 106 *vs.* 108, respectively.

Finally, we note specifics of interest concerning several stars. (1) BX Dra was shown by Schmidt *et al.* (1995) to be an eclipsing binary rather than an RR Lyrae (Kholopov 1985); it was removed from our database. (2) L94 found SV Boo to have [Fe/H] = –0.43 from a single low-quality spectrum, whereas Hemenway (1975) quoted $\Delta S = 7$ ([Fe/H]$_{L94}$ = –1.55). Since the kinematics of SV Boo suggest it belongs to the halo, we adopt the Hemenway abundance. (3) The radial velocity of BB Pup was revised to 98 ± 9 km s^{-1} from that in L94 by eliminating the outlier velocity 255 ± 16 km s^{-1} from the list in Table 2 of L94. (4) For three stars, AE Dra, BD Dra, and BK Eri, the proper motion was improved by removing one discordant measurement from the average value quoted in the NPM1 Catalog. (5) The seven stars listed with the abundance source "3" in Table 2 all had photometrically-determined [Fe/H] values from Hemenway (1975; see Sec. 2.2) which suggested that they were thick disk stars. However, their kinematics suggested that all seven stars are halo members. We therefore set [Fe/H] = –1.5 for these stars. (6) We found that RX CVn historically has been misidentified. The proper motion of WMJ and the radial velocity of Joy (1950) give a space velocity greater than the escape velocity of the Galaxy. The NPM proper motion and the radial velocity measured by L94 (see our Table 2) give a reasonable space velocity for a halo star. Inspection of the NPM plates shows that the measured star has a nearby companion, probably a foreground dwarf, which was probably mistakenly observed by WMJ and Joy. The RR Lyrae is the eastern-most of the pair.

3. Kinematics and Population Separation

Layden (1995, hereafter referred to as L95) showed that the RR Lyraes separate into a halo and a (primarily thick) disk population at [Fe/H] = –1.0. We wish to see if this separation persists using our improved database.

To do this, we computed provisional distances to the stars in our sample using the $M_V(RR)$–

[Fe/H] relationship of Carney, Storm & Jones (1992, hereafter referred to as CSJ), $M_V(RR) = 0.15[\mathrm{Fe/H}] + 1.01$ mag. We then computed the stars' U, V, W space velocities, following Johnson & Soderblom (1987) with one exception: we take U as positive outward. At distances of 1–2 kpc, typical of the distances in our sample, the Sun-oriented U, V, W frame can be misaligned by a small angle in the U, V plane ($RMS \approx 6$ deg) from the cylindrical Galactic directions (π, θ, z) at each star. So, we rotated the U, V, W velocities into the π, θ, z frame, after adding to V the IAU standard rotational velocity $\Theta_0 = 220$ km s^{-1} (Kerr & Lynden-Bell 1986), and after adding the "dynamical" solar motion (–9, +12, +7 km s^{-1}; Mihalas & Binney 1981, p.400) to correct U, V, W to the Local Standard of Rest (LSR). The results are the velocity components V_π, V_θ, and V_z, where V_π increases outwards from the axis of Galactic rotation, V_θ increases in the direction of Galactic rotation, and V_z increases toward the North Galactic Pole.

Figure 3 shows V_π and V_z plotted against V_θ. Clearly, the stars with [Fe/H] < –1.0 have large velocity dispersions and little net Galactic rotation, typical of the halo. Meanwhile, the stars with [Fe/H] > −1.0 are clustered around $V_\theta \approx 200$ km s^{-1}. Figure 4 shows V_θ as a function of abundance.

While the distribution of stars in Figures 3 and 4 is consistent with the first-order view of a disk/halo separation at [Fe/H] = –1.0, there are four stars with $V_\theta < 60$ km s^{-1} at [Fe/H] > −1.0, whose extreme kinematics clearly mark them as members of the halo. Similarly, there may be an excess of stars with $V_\theta > 80$ km s^{-1} at [Fe/H] < −1.0, which may belong to the "metal-weak thick disk" (MWTD; Morrison, Flynn & Freeman 1990). L95 discussed the presence of such stars in his sample of RR Lyraes.

It is not possible to assign these stars individually to the disk or halo populations without ambiguity. We therefore separate the disk from the halo using three distinct definitions, and perform the stat-π solutions for each set of definitions, in order to test the effects of the different definitions on the derived kinematics and absolute magnitudes.

The three disk/halo separation definitions are summarized in Table 3. All three definitions assign the four low-V_θ stars with [Fe/H] > −1.0 to the halo. The first definition, similar to that of Nissen & Schuster (1991), admits a small number of MWTD RR Lyraes, primarily with −1.3 < [Fe/H] < −1.0, in agreement with L95. The second assumes that no MWTD ([Fe/H] < −1.0) RR Lyraes exist. The third definition admits a larger population of MWTD RR Lyraes, which reaches to [Fe/H] ≈ −1.6, more along the lines of the population of red giants described by Morrison *et al.* (1990). Two stars, AO Peg and FU Vir, fit one or more of the disk definitions, yet clearly belong to the halo based on their extreme kinematics: (V_π, V_θ, V_z) = (–212, +236, –207) and (–178, +249, –93), respectively. We have moved these stars into the corresponding halo definitions, as noted in Table 3.

We note that the choice of $M_V(RR)$–[Fe/H] relations used to compute the distances does not significantly affect the separation. Only one star crosses the sloping disk/halo line in Fig. 4 when we change from the CSJ $M_V(RR)$–[Fe/H] relation to that advocated by Sandage (1993).

4. Monte Carlo Simulations

4.1. Testing the Stat-π Algorithm

In Sec. 5 we will present the stat-π analysis of our data. First, however, we will test the HJBW stat-π algorithm itself, using synthetic data with known properties (positions, velocities, $M_V(RR)$, etc.). This step seems vital to ensure reliable results. Specifically, we test: (1) how accurately the stat-π solutions reproduce the kinematics and luminosities of the input data; (2) how reliable the error estimates are; (3) the sensitivity to the number of stars and their distribution on the sky; (4) whether all the free parameters in the HJBW stat-π algorithm are necessary; (5) whether the small misalignment (Sec. 3) between U, V, W and V_π, V_θ, V_z has any significant effects; (6) whether the results are biased by any input assumptions; and (7) whether any corrections are necessary for bias in the results.

The HJBW algorithm uses a simplex optimization technique to maximize the likelihood in Murray's (1983) kinematic model (also used by SRM). There are 11 free parameters: the solar motion (U, V, W), the velocity ellipsoid $(\sigma_U, \sigma_V, \sigma_W)$ with three covariances $(\sigma_{UV}, \sigma_{UW}, \sigma_{VW})$ to allow an arbitrary orientation, the distance scale parameter k and its dispersion σ_k. The solution also returns an approximate standard error estimate σ_i for each parameter. The solution returns an absolute magnitude M_V by differential correction to a starting value M_A, which for convenience we fix at +1.0. We refer the reader to HJBW for full details of the stat-π algorithm. We made two modifications to the HJBW procedure: (1) we fixed an error which caused the large velocity dispersion errors listed in Table 2 of HJBW; and (2) when necessary, we inspected the data to reject extreme outliers and repeated the solutions.

4.2. Simulated Data Sets

To perform Monte Carlo tests we generated an ensemble of simulated data sets as outlined in Table 4. These were designed to realistically simulate the halo and disk subsamples of our real data (Sec. 3).

For the halo and disk simulations H1 and D1, $N_{stars} = (165,\ 50)$ were randomly assigned spatial positions (X, Y, Z) and [Fe/H] values from uniform distributions with appropriate limits. M_V values were then computed from the $M_V(RR)$–[Fe/H] relation of CSJ, with a Gaussian cosmic dispersion $\sigma_M = 0.2$ mag. Space velocities (V_π, V_θ, V_z) were generated from a Gaussian velocity ellipsoid whose parameters are given in Table 4. Each star's right ascension, declination, proper motion, radial velocity, and apparent magnitude were then calculated, with Gaussian observational errors 0.5 arcsec cen^{-1} and 20 km s^{-1} added to the proper motion components and the radial velocity, respectively. For each simulation (H1, D1) we created $N_{trials} = (5,\ 20)$ different data sets; N_{trials} was set larger for the disk simulations because N_{stars} is proportionately smaller.

As discussed in Sec. 2, the actual distribution of our RR Lyraes on the sky is far from uniform.

To test whether this affects the stat-π results, we prepared alternate data sets (H2, D2) using the observed sky positions, apparent magnitudes, and metallicities from Table 2, with the Disk-1/Halo-1 separation of Table 3. Then, N_{trials} sets of synthetic proper motions and radial velocities were randomly generated as above.

For each data set (H1, H2, D1, D2), stat-π solutions were performed as outlined in column 6 of Table 4. Multiple solution sets tested particular parameters in the HJBW model. To test the effect of the HJBW distance scale dispersion parameter σ_k we ran two solutions for each halo data set, with $\sigma_k = (0.0, 0.1)$ as indicated in column 7 of Table 4. These solutions will be discussed in Sec. 4.6. For the data sets H2 and D2 we ran solutions with and without the velocity covariance parameters $(\sigma_{UV}, \sigma_{UW}, \sigma_{VW})$, as indicated in column 8 of Table 4. The reasons for this will be discussed in Sec. 4.7. Fifteen additional H2 data sets (row 5 of Table 4) were created in order to test with higher precision the important solution sets which excluded the velocity covariance parameters. The significance of these solutions will be discussed in Sec. 4.8. Finally, we note that for a few of the disk data sets, the solutions failed to converge ($N_{conv} < N_{trials}$). This will be discussed in Sec. 4.5.

4.3. Coordinate Frame Misalignment

Before discussing the stat-π solutions, we need to deal with an apparent inconsistency between the data simulations and the HJBW solution method. We generated our simulated velocities using velocity ellipsoids oriented to the cylindrical coordinate frame (V_π, V_θ, V_z) which is physically the most appropriate frame for Galactic velocities. However, the HJBW algorithm uses the (U, V, W) rectangular coordinate frame to compute the solar motion and stellar velocity dispersions. In Sec. 3, we noted that the (U, V, W) coordinates can be misaligned with (V_π, V_θ, V_z), by a small angle (RMS $\sim$ 6 deg). It is important to show that any effects of this misalignment are too small to significantly affect our results.

We can do this directly with the simulated data, because for every star we know the space velocity in each coordinate frame. This lets us measure, for every data set, any differences (1) between $\langle U, V, W\rangle$ and $\langle V_\pi, V_\theta, V_z\rangle$ and (2) between $\sigma_{(U,V,W)}$ and $\sigma_{(\pi,\theta,z)}$. In the remainder of this paper, we refer to the values computed directly from the simulated data as the "true" values for the data set.

For the halo (H1, H2), the principal effect is the projection of the long axis of the velocity ellipsoid (σ_π) partly onto the V axis, increasing σ_V at the expense of σ_U. Quantitatively, $\sigma_U = \sigma_\pi - 0.4$ km s^{-1}, and $\sigma_V = \sigma_\theta + 0.5$ km s^{-1}. Clearly, these effects are far too small to be of any concern here.

For the disk (D1, D2), the principal effect of coordinate misalignment is the partial projection of the rotation vector $V_\theta = 200$ km s^{-1} onto the U axis. Distant stars in the direction of Galactic rotation $(l, b) = (90, 0)$ get a negative contribution to their U velocity; stars toward (270,0) get

a positive contribution. The net effect is that $\sigma_U = \sigma_\pi + 3$ km s^{-1}. Also, $\langle V \rangle$ is decreased by 1 km s^{-1}. Again, these effects are considerably smaller than the observational errors, and can be neglected in practice.

4.4. Monte Carlo Simulation Results

Stat-π solutions for each of the 25 halo and 40 disk data sets were performed as outlined in Table 4. The results for each set of solutions are summarized in Table 5. The left side of Table 5 gives results for the V component of the solar motion, the three velocity dispersions $(\sigma_U, \sigma_V, \sigma_W)$, and M_V. The Δ values on the right side of Table 5 represent the differences (solution $-$ "true") for each quantity. Table 5 omits the U and W solar motion components, as these were always equal to the true values to $\lesssim 1$ km s^{-1}.

Each solution set in Table 5 lists two rows of results. The first row gives the mean of each quantity. The second row gives two different estimates of the uncertainty in the quantity: $\langle \sigma_i \rangle$ (left side of Table 5) gives the mean of the internal error estimates returned by the HJBW code for each parameter, while SD (right side) gives the RMS dispersion about each mean difference. The latter external error estimates reflect how precisely the stat-π program returns the "true" values. The values in row 5 of Table 5 are more precise than those quoted for the other halo simulations, since they are based on 20 rather than 5 data sets.

The major result of the Monte Carlo simulations is that the HJBW algorithm does an excellent job of returning the "true" input parameters, to within a few km s^{-1} for the velocities and dispersions, and to within ~ 0.1 mag for M_V. This is true for both the halo and the disk simulations, and for both the random and real space distributions. Furthermore, in nearly all cases the external errors (SD's of the Δ's) are no larger than the HJBW program's internal error estimates $\langle \sigma_i \rangle$, and in some cases they are considerably smaller.

Detailed examination of Table 5 shows some small systematic effects which are worth considering further. Note that 7 out of 8 $\langle \Delta V \rangle$ values are positive, all 24 $\langle \Delta\sigma \rangle$ values are negative, and 7 out of 8 $\langle \Delta M_V \rangle$ values are positive. Examination of the individual solutions shows that these same effects occur on a solution-by-solution basis, with V, $\sigma_{(U,V,W)}$, and M_V all varying in tandem, linked together by the HJBW distance scale parameter k. The average values are slightly biased toward a "short" distance scale ($k < 0$, $\Delta M_V > 0$). This bias is larger for the real space distribution data sets (H2, D2) than for the random sets (H1, D1). Whether we can or should correct for this small bias will be discussed in Sec. 4.8.

For the halo (H) solutions, the internal error estimates $\langle \sigma_i \rangle$ returned by the HJBW program tend to be larger than the external errors. For example, $\langle \sigma_i \rangle$ for M_V is 0.12 mag, while the SD of ΔM_V averages 0.08 mag. For the kinematic parameters, $\langle \sigma_i \rangle$/SD $\gtrsim 2$. These results indicate that the real accuracy of the halo solutions may be better than the internal errors claim. However, given the simplified nature of the simulations, we will conservatively adopt the internal error estimates

in discussing our real data solutions (Sec. 5).

For the disk (D) solutions, the internal and external errors for M_V generally agree, though there is a small discrepancy for the kinematic parameters, $\langle\sigma_i\rangle$/SD ≈ 1.4. In addition, the standard error of M_V is ∼0.3 mag, 3–4 times as large as for the halo. The failure of the M_V errors to follow an $N^{-1/2}$ relation may mean that $N_{stars} = 50$ is near the lower limit for successful solutions (see Sec. 4.5), but it must also reflect the fact that the stat-π method inherently works better for a population with a larger velocity dispersion.

The test solutions (H1.0, H2.0) with the HJBW distance scale dispersion parameter σ_k set to zero will be discussed in Section 4.6. The test solutions (H2d, D2d) without the velocity ellipsoid covariances $(\sigma_{UV}, \sigma_{UW}, \sigma_{VW})$ will be discussed in Section 4.7.

4.5. Sample Size and Solution Convergence

Since the number of stars in our disk samples (both real and synthetic data) is near or below the lower limit (50 stars) that HJBW found necessary for successful solutions, we need to ask how reliable our disk solutions can be with so few stars. The symptom of having too few stars is that the HJBW likelihood function becomes ill-conditioned, and the iterative solution fails to converge to finite output parameters (hence $N_{conv} < N_{trials}$ in Table 4).

Surprisingly, given the HJBW result, over 90% of our Monte Carlo disk solutions, and all 3 real-data disk solutions (Sec. 5) did in fact converge. Moreover, Table 5 shows that the disk output parameters are well-determined, i.e., they have little bias and accurate error estimates. The convergence of our Monte Carlo solutions for $N_{stars} \leq 50$ may reflect the Gaussian nature of our simulations, in contrast to the vagaries of the real data that HJBW used. In our experience, the HJBW algorithm is not resistant to large outliers; for real data, this makes the disk/halo separation quite critical. The success of our real-data disk solutions for $N_{stars} \simeq 40$ is most likely due to the better separation we achieved using [Fe/H] and V_π (Sec. 3, Fig. 4) instead of ΔS and period (HJBW).

Without doing many more simulations, it is not possible for us to state what the true lower limit on N_{stars} may be. Nor is this necessary, since the clear result of our Monte Carlo simulations is that solutions that do converge give reliable results.

4.6. Effects of Cosmic Dispersion in $M_V(RR)$

Both HJBW and SRM found a strong correlation in their stat-π solutions between $M_V(RR)$ and σ_M, the cosmic dispersion in $M_V(RR)$. In the Murray (1983) model, the cosmic dispersion is parameterized by σ_k, the dispersion in the distance scale parameter k. This correlation effectively prevents solving for σ_k; instead this parameter must be fixed at a value chosen to represent a

reasonable value of σ_M. Equation 8 of HJBW relates σ_M, σ_k, and k. For $\sigma_k = 0$, $\sigma_M = 0$. For $\sigma_k = 0.1$ and $\langle k \rangle = -0.1$ from our solutions, $\sigma_M \simeq 0.24$ mag.

Observations show this to be a reasonable range of σ_M. Sandage (1990a) found the intrinsic dispersion of RR Lyrae magnitudes within a globular cluster (i.e., at a single metallicity) to be σ_V = 0.06–0.15 mag. For our field RR Lyraes there will be an additional dispersion σ_s proportional to the slope of the $M_V(RR)$–[Fe/H] relation. We estimated σ_s numerically by populating various $M_V(RR)$–[Fe/H] relations with "stars" having the [Fe/H] distribution of our halo sample. The total σ_M is then the quadratic sum of σ_V and σ_s. For $\sigma_V = 0.1$ mag, using the CSJ $M_V(RR)$–[Fe/H] relation (slope = +0.15 mag dex^{-1}) we obtain $\sigma_M = 0.11$ mag. Using the steeper slope (+0.39) advocated by Sandage (1990b) gives $\sigma_{Mv} = 0.17$ mag. To reach $\sigma_{Mv} = 0.24$ mag, we must adopt an extreme value of $\sigma_V = 0.2$ mag along with the Sandage (1990b) slope.

Consequently, a reasonable range of σ_k to test in our Monte Carlo solutions is $0.0 \leq \sigma_k \leq 0.1$. Solution sets (H1.0, H1) and (H2.0, H2) with $\sigma_k = (0.0,\ 0.1)$ respectively (Table 4) let us evaluate the effects on $M_V(RR)$. The results in Table 5 indicate that $M_V(RR)$ comes out ∼0.03 mag brighter for $\sigma_k = 0.1$ than for $\sigma_k = 0.0$. Similar results were found by HJBW and SRM. Table 5 shows that the assumed value of σ_k does not affect the derived kinematics. Clearly, our choice of σ_k will only have a small effect on our stat-π results. To be conservative, we will adopt $\sigma_k = 0.1$ to analyze our real data (Sec. 5). For a given solution the true value of $M_V(RR)$ thus may be a few hundredths of a magnitude fainter than the value we derive.

4.7. Velocity Ellipsoid Covariances

Three of the 11 parameters in the Murray (1983) model are the covariances $(\sigma_{UV}, \sigma_{UW}, \sigma_{VW})$ which allow the velocity ellipsoid to have an arbitrary orientation with respect to the principal Galactic directions. The results of HJBW strongly suggest that this may not be necessary in practice. Given the apparent benefits of eliminating unneeded parameters from the model (especially for the disk, where $N_{stars} \lesssim 50$ does not greatly exceed the number of free parameters), it seems wise to use our Monte Carlo simulations to test whether the covariances $(\sigma_{UV}, \sigma_{UW}, \sigma_{VW})$ are needed in our real-data stat-π solutions.

Because our simulated data were generated with no correlations among the (U, V, W) velocities, the covariances $(\sigma_{UV}, \sigma_{UW}, \sigma_{VW})$ returned by the stat-π solutions simply reflect random scatter in the data. Thus the covariances for the real-data solutions can be tested for statistical significance by comparison with the Monte Carlo simulations.

To do this, for each stat-π solution we calculated the correlation coefficients (CC's) $\rho_{UV} = \sigma_{UV}/\sigma_U\sigma_V$, etc. For each of the sets of simulated data listed in Table 4, we computed the mean, SD, and range of the CC's of the individual trials. For all the simulations, the mean correlations were near zero, as expected. For the halo, (both H1 and H2) each of the three SD's was $\lesssim 0.1$. By comparison, the RMS value of the real-data halo CC's was 0.10, with none of the CC's exceeding

the range of the simulated values. For the disk, the SD's were ~ 0.2 for set D1 (random space distribution), and ~ 0.3 for set D2 (real space distribution). The RMS value of the real-data disk CC's was 0.13; again none of the CC's exceeded the range of the simulated values.

From these tests we conclude that there is no evidence, for either the halo or the disk RR Lyraes, that the velocity ellipsoid deviates from the principal directions (U, V, W). Consequently, we can run our stat-π solutions with the covariance parameters $(\sigma_{UV}, \sigma_{UW}, \sigma_{VW})$ removed from the model. The entries in Table 5 for solution sets H2d and D2d show the results of these solutions on the data sets H2 and D2. There is little difference in the kinematics or absolute magnitudes produced by the new solutions, save for a slight tendency for the errors to be reduced. Analyzing our real data (Sec. 5) without the unneeded covariances reduced the disk M_V errors by 10%.

4.8. Bias Corrections

In Sec. 4.4 we found that the results in Table 5 suggested that the stat-π solutions may be slightly biased toward a "short" distance scale. The solution velocities are consistently several per cent too small, and $M_V \lesssim 0.1$ mag too faint. The bias was largest ($\langle \Delta M_V \rangle = +0.13$ mag) for the data set D2, the disk simulation with the space distribution of the real RR Lyraes. Although this bias is much less than the random error (~ 0.3 mag) of a single disk solution, it may still be worth applying corrections to our real-data results (Sec. 5).

The above-mentioned bias toward a "short" distance scale should not be confused with a bias toward the *fainter* M_V regime discussed in Secs. 1, 6, and 7 (i.e., toward $M_V(RR) \approx +0.7$ mag at [Fe/H] ≈ -1.6, rather than +0.4 mag). It can easily be demonstrated that our solutions have no intrinsic bias toward any particular M_V value; nor are the solutions biased by the choice of the starting value M_A. Tests using simulated data sets based on $M_V(RR)$ 0.5 mag brighter than the CSJ relation adopted in Sec. 4.2 correctly returned M_V values 0.5 mag brighter, with unchanged kinematics. These results were recovered exactly when a brighter starting value $M_A = +0.5$ was used, and to within ~ 0.01 mag in M_V and $\sim 1\%$ in the velocities even when the usual $M_A = +1.0$ was used.

In the spirit of exploratory data analysis, we plotted ΔM_V versus the "solution" and "true" values of the velocities (U, V, W) and dispersions $\sigma_{(U,V,W)}$ for all 65 simulations. This led to the discovery that, for the real space distribution sets (H2, D2), the bias was smallest when the velocity ellipsoid was "long", i.e. when $\sigma_U \gg \sigma_V$, and largest when the velocity ellipsoid was "round", i.e. when $\sigma_U \lesssim \sigma_V$. Thus the disk is chiefly affected, while the halo is not. The 15 additional H2d solutions outlined in Table 4 were performed to illuminate this situation.

Figure 5 plots ΔM_V as a function of $\sigma_U(true)/\sigma_V(true)$ for solution sets H2d and D2d. Because of their markedly different distributions on the sky, we consider the halo and disk separately in Fig. 5. For the halo, the small bias ($+0.036 \pm 0.019$ mag) is well-determined because of the increased number of H2d solutions, but the slope is not statistically significant. For the disk, both the mean

bias (+0.13 mag) and the slope (–0.69 mag) are 2-σ significant.

We suggest that these results may be used to apply a bias correction (subtracted from M_V) to our real-data results (Sec. 5) for the disk, as a function of σ_U/σ_V. (We choose not to apply a ΔM_V correction to the halo results for two reasons. The halo correction would be small compared to the other sources of error in $M_V(RR)$ discussed in Sec. 6; moreover the bias is compensated by the roughly equal, but opposite, σ_k effect discussed in Sec. 4.6.) For consistency, when we apply the disk ΔM_V correction in Sec. 5, we will also correct the disk kinematics for the "short" distance scale by enlarging the velocities and dispersions by a factor of $10^{0.2\ \Delta M_V}$.

Two objections may be raised to these corrections: first, that the reason for the bias is not understood, and second, that the "true" value of σ_U/σ_V is not known for the real data. The latter problem can be overcome by computing σ_U and σ_V directly from the data, as in Sec. 3. Because we only need the ratio σ_U/σ_V, any distance dependence from the assumed $M_V(RR)$–[Fe/H] relation cancels out.

It remains mysterious to us why the disk stat-π solutions are slightly biased when the velocity ellipsoid is "round". Since the effect occurs for the real (but not a random) stellar distribution, it must be caused by the the uneven distribution of the disk RR Lyraes on the sky. It might be possible to solve this puzzle with a much larger set of simulations, but that is clearly beyond the scope of this paper. We note that maximum-likelihood methods in general are not unbiased; Clube & Dawe (1980a) found an equal M_V bias (-0.12 mag) in the opposite direction! We conclude simply that since our disk M_V bias is relatively large and can be calibrated as a function of the observational variables, we should apply it to our real-data solutions.

5. Stat-π Solutions for Observed RR Lyrae Data

Applying the lessons learned from our Monte Carlo simulations (Sec. 4), we analyzed our real data (each of the Disk/Halo subsamples in Table 3) by running the stat-π program with $\sigma_k = 0.1$ and performing two sets of solutions, with and without the velocity ellipsoid covariances $(\sigma_{UV}, \sigma_{UW}, \sigma_{VW})$. As in Sec. 4.7, the differences between the two sets of solutions were small. The kinematics generally changed by < 1 km s^{-1}; M_V averaged $\sim$ 0.02 mag brighter in the solutions without the covariance terms. Most important, the errors returned by the stat-π program for the disk data sets were typically 10% smaller without the covariances, presumably owing to the larger number of degrees of freedom attained by removing three free parameters from the solutions. Since the correlation coefficients $(\rho_{UV}, \rho_{UW}, \rho_{VW})$ did not prove to be significant (Sec. 4.7), we therefore adopt these solutions, with the velocity ellipsoid aligned to the principal Galactic directions (U, V, W), as our final results.

Table 6 presents, for each solution as discussed below, the solar motion $\langle U, V, W\rangle$, the velocity ellipsoid $\sigma_{(U,V,W)}$, and the absolute magnitudes. Below each of these entries is presented the standard error for that term, computed by the stat-π program. Recall that the Monte Carlo simulations

suggested that the true uncertainties may be as much as 2 times *smaller* than those quoted in the table. The final column of Table 6 shows the $M_V(RR)$ values after correction for the σ_U/σ_V bias discussed in Sec. 4.8.

5.1. Kinematic Results

Examination of Table 6 shows that the kinematics of the RR Lyraes do not depend significantly on which disk/halo definition is employed. Because Definition 3 of Table 3 gives the purest halo sample and the largest, best-determined disk sample, we adopt Halo-3 and Disk-3 as our best solutions in Table 6. Thus, our best estimates of the net rotation and velocity ellipsoid of the halo RR Lyraes are

$$\langle V \rangle = -210 \pm 12 \text{ km s}^{-1}, \quad V_{rot} = 22 \pm 12 \text{ km s}^{-1}$$

$$(\sigma_U, \sigma_V, \sigma_W) = (168 \pm 13,\ 102 \pm 8,\ 97 \pm 7) \text{ km s}^{-1}.$$

For the disk RR Lyraes, after correcting (by a factor of 1.07) for the distance scale bias ($\Delta M_V =$ +0.15 mag, Sec. 5.2), we obtain

$$\langle V \rangle = -48 \pm 9 \text{ km s}^{-1}, \quad V_{rot} = 184 \pm 9 \text{ km s}^{-1}$$

$$(\sigma_U, \sigma_V, \sigma_W) = (56 \pm 8,\ 51 \pm 8,\ 31 \pm 5) \text{ km s}^{-1}.$$

We note (see Sec. 4.4) that the HJBW stat-π program implicitly accounts for the effects of observational errors in the determination of the velocity dispersion parameters, so these results are unbiased estimates of the true velocity dispersions of the halo and disk RR Lyrae populations.

These kinematic values are in excellent agreement with the RR Lyrae kinematics derived by L95. They also correspond quite well with the kinematics of the thick disk and halo based on other tracer populations (*cf.* Casertano *et al.* 1990; L95 Table 8), with two possible exceptions. First, the vertical velocity dispersion of the disk, $\sigma_W = 31$ km s^{-1}, is somewhat smaller than the typically quoted value of 35–45 km s^{-1}. L95 suggested that the RR Lyrae "disk" subsample contains stars from both the thick disk and the old thin disk populations, such that the net kinematics are intermediate between the two. Unfortunately, the disk sample contains too few stars for us to subdivide it and perform meaningful stat-π solutions for separate thin and thick disk components.

Second, σ_U for the halo RR Lyraes is large compared to many other estimates, 168 km s^{-1} *vs.* 120–155 km s^{-1}. The cause of this effect is less clear. It may be due to our removing interloper thick disk stars more completely than other studies (L95), or it may be related to a subtle selection bias experienced by RR Lyraes. For example, if the halo is composed of an accreted component and a dissipatively-formed component (Zinn 1993, Majewski 1993), if the components have different kinematics (e.g., Beers 1996), and if RR Lyraes are more easily formed in one component than the other, then using RR Lyraes as kinematic tracers would bias the kinematic results to favor one or the other halo components, relative to their representation in samples using other stellar

tracers. At present, it seems that the halo RR Lyraes may be preferentially tracing the accreted halo component, though a detailed analysis outside the scope of this paper is required to further address this problem.

5.2. Absolute Magnitudes

In Table 6, M_V is virtually the same for each of the three halo definitions. As above, we adopt Halo-3 as our purest definition of the halo RR Lyraes. This gives

$$M_V(RR) = +0.71 \pm 0.12 \text{ mag} \quad \text{at} \quad \langle[\text{Fe/H}]\rangle = -1.61.$$

As discussed in Secs. 4.8 and 6, no bias corrections have been applied to the halo solutions.

For the disk, M_V is more sensitive to which set of stars is used in the stat-π solution. As in the Monte Carlo simulations (Sec 4.4), the errors in the derived M_V's for the disk are ~ 3 times larger than for the halo. Both effects are largely due to the relatively small number of stars in the disk solutions. Again we adopt Disk-3 as the best solution. Since the disk velocity ellipsoid is quite "round" ($\sigma_U(true)/\sigma_V(true) = 1.06$), a bias correction of +0.15 mag (Figure 5) was subtracted from the solution value, giving

$$M_V(RR) = +0.79 \pm 0.30 \text{ mag} \quad \text{at} \quad \langle[\text{Fe/H}]\rangle = -0.76.$$

5.3. Effects of Disk/Halo Separation

To see what would have happened had we been unable to separate the disk and halo RR Lyraes, we performed a stat-π solution (last line of Table 6) using all 213 stars. This solution is comparable to "Group RR *ab*" of HJBW (142 stars) and to "Sample C′" (139 stars) of SRM. Interestingly, the absolute magnitude ($+0.73 \pm 0.11$) for our "All stars" solution is almost exactly the same as for the three halo solutions, but the kinematics are rather different. For this mixture of disk and halo, $\langle V\rangle$, σ_U, and σ_W are smaller than for the pure halo, but σ_V is larger. The velocity ellipsoid is much "rounder"; $\sigma_U/\sigma_V = 1.28$, vs. 1.65 for Halo-3. HJBW and SRM found $\sigma_U/\sigma_V = 1.25$ and 1.29, respectively, for the comparable groups.

These results point out that a good disk/halo separation is necessary to get reliable kinematic results for the RR Lyraes. The stat-π method is robust enough to produce solutions for mixed populations with distinctly different kinematics, successfully determining M_V, but it derives kinematics not accurately representing either population.

5.4. $M_V(RR)$ Variations with [Fe/H]

The fact that we have separate disk and halo solutions over a range of almost 1 dex in [Fe/H] gives hope that we might obtain the slope of the $M_V(RR)$–[Fe/H] relationship, a parameter of considerable astrophysical importance (Sec. 1) which previous stat-π studies (e.g., HJBW, SRM) found difficult to determine. Unfortunately, our disk solutions are not sufficiently precise to meaningfully constrain this slope. Figure 6 depicts this fact graphically; the error bars on the disk solutions easily admit slopes between 0 and +0.4 mag dex^{-1}, the extreme values currently under debate. Calculating the slope using the bias-corrected $M_V(RR)$ estimates for Halo-3 and Disk-3 from Table 6, we obtain $\Delta M_V \ / \ \Delta[\mathrm{Fe/H}] = +0.09 \pm 0.38$ mag dex^{-1}.

To pursue the $M_V(RR)$–[Fe/H] slope further, we divided the Halo-1 sample at [Fe/H] = –1.55, giving equal-sized metal-rich and metal-poor sub-groups. We performed stat-π solutions on each group (Halo-1R and Halo-1P in Table 6, and the crosses in Figure 6). These solutions show no indication of any slope within the halo. Again, we are unable to constrain the slope of the $M_V(RR)$–[Fe/H] relation within meaningful limits.

In a final effort to determine the $M_V(RR)$–[Fe/H] slope, we attempted to incorporate this dependence directly into the stat-π program by parameterizing the absolute magnitude term M_A in Eqn. 5 of HJBW with with two coefficients a and b, where

$$M_A \ = \ a([\mathrm{Fe/H}] - \langle[\mathrm{Fe/H}]\rangle) \ + \ b.$$

However, preliminary solutions indicate that this makes the maximum-likelihood solution ill-conditioned. It may be possible to avoid this problem by incorporating the [Fe/H] dependence into the distance scale correction k rather than M_A; we are continuing to work on this problem, and any results will be reported in a future paper.

6. Comparisons with other Measurements

In Sec. 1, we mentioned the long history of efforts to determine $M_V(RR)$. CSJ provide an extensive review of much of this work, which we shall not repeat here. Table 7 presents the results of some of these efforts [2]. They are plotted as a function of [Fe/H] in Figure 7 to facilitate comparison with the results of our stat-π solutions. We refer the interested reader to the individual references in Table 7 for more detailed discussions on these methods.

We begin by noting that our stat-π solutions are in good agreement with the results of the two recent applications of the method ($M_V(RR)$ = +0.68, BH86; $M_V(RR)$ = +0.75, SRM). This is

[2] The $M_V(RR)$ values produced by the stat-π method are for "typical" RR Lyraes in the sample. These stars tend to be somewhat evolved off the Zero Age Horizontal Branch (ZAHB). Some $M_V(RR)$ estimates using different methods refer to $M_V(RR)$ at the ZAHB. We note these cases in Table 7, where we have corrected $M_V(ZAHB)$ to $M_V(RR)$ using the Eqn. 4 of CSJ.

not a complete surprise, given that the stars in those studies are all included in the present study, albeit with improved data. As shown in Table 7 and Figure 7, the agreement between the various stat-π solutions becomes even better when small corrections are made to bring the previous results onto the system of reddenings and magnitudes used in this paper. Like us, neither of the previous groups was able to detect a meaningful trend in $M_V(RR)$ with [Fe/H] due to the small sample sizes.

At the characteristic abundance of the halo, [Fe/H] ≈ -1.6, the various results shown in Figure 7 cover a range of 0.2–0.3 mag, and appear to separate into a brighter and a fainter group. Interestingly, whether a particular result is bright or faint does not seem to be a function of the method employed. For example, Buonanno *et al.* (1990) found a bright zero-point by fitting 19 globulars to 5 subdwarfs, while CSJ found a faint zero-point by fitting a single cluster to the subdwarf (of identical abundance) with the best trigonometric parallax. Similarly, using the Sandage period-shift effect, Sandage (1990b) obtained a bright zero-point and a steep slope. Using data for a different set of field stars, adopting a different effective temperature relation, and employing a different mass-metallicity relation, CSJ obtained a moderate slope. Fernley (1993) used infra-red rather than optical observations of field and cluster RR Lyraes in his period shift analysis, and found a bright zero-point but a moderate slope. Apparently, the current uncertainty in $M_V(RR)$ is dominated by differences in the details of the methods a particular author follows, and his or her choice of a particular data set or reddening correction. It is very difficult to determine which of these assumptions are correct or incorrect at this level of detail.

In deciding which methods shown in Figure 7 should be given the most weight, it is worth noting several strengths of the stat-π method. First, stat-π is independent of other distance determinations. By contrast, cluster main sequence fitting requires precise trigonometric parallaxes to the nearby subdwarfs. Calibrations of $M_V(RR)$ based on LMC distances determined by other methods are similarly complicated. For example, the Cepheid calibration used by Walker (1992) to obtain the LMC distance is based on main sequence fits of Cepheid-bearing Galactic open clusters to the Pleiades, *and* main sequence fits of the Pleiades to local dwarfs with trigonometric parallaxes.

A second strength of the stat-π method is that it relies on a simple, extremely well-tested model. The kinematics of the Galaxy are described by three mean velocities, three velocity dispersions, and the orientation of this velocity ellipsoid relative to the cardinal directions of the Galaxy. Countless kinematic studies over the past half century have shown this to be a very complete description of local Galactic kinematics.

By comparison, the models or basic assumptions on which many of the other techniques rely are far more complex, and tend not to be so well-tested. For example, the Baade-Wesselink method depends on model atmospheres to determine both the surface brightness constant, S_o, and the observed-to-pulsation velocity correction, p (Jones *et al.* 1992). Both the Baade-Wesselink and period shift methods rely on a color-index *vs.* effective temperature relation, and different authors advocate different relations (Sandage 1990b, CSJ, Fernley 1993, Sandage 1993). The period

shift method also relies heavily on the assumed RR Lyrae mass-metallicity relation, yet the mass estimates from double-mode RR Lyraes are in serious conflict with those derived from the Baade-Wesselink method, and to a lesser extent with masses derived from HB theory (Fernley 1993, Yi *et al.* 1993). Meanwhile, $M_V(RR)$ estimates from HB theory are dependent on the color–temperature relation, the evolutionary models (including the treatment of convection), and especially on the assumed main sequence helium abundance, Y_{MS} (Lee 1990). $M_V(RR)$ values derived from main sequence fits currently rely on theoretical isochrones to correct the colors and/or magnitudes of the clusters and/or field subdwarfs to a common metallicity (Buonanno *et al.* 1990, Bolte & Hogan 1995). The reader is referred to the papers noted above and in Table 7 for detailed discussion of these topics.

Our $M_V(RR)$ result for the halo is 0.06 mag brighter than the CSJ value at [Fe/H] = −1.61, and agrees better with this and other "faint" $M_V(RR)$ values than the "bright" results shown in Fig. 7, which are ∼0.2 mag brighter. Given this dichotomy, it is valid to ask whether there are any parameters we could change that would push our result to a brighter value. The results of SRM suggest that if we adopted the Sturch (1966) reddening scale, based on the blanketing-corrected colors of RR Lyraes at minimum light, we would obtain a result ∼0.11 mag *brighter* than our current result. However, SRM argue that the Burstein & Heiles (1982) H I based redding scale is preferred.

In Sec. 2.4, we noted that the various sources of RR Lyrae photometry suffer small inconsistencies in photometric standardization at the 0.07 mag level. Had we used the un-transformed literature values, we would have obtained an $M_V(RR)$ for the halo about 0.07 mag *fainter*.

Several other effects could alter our $M_V(RR)$ result by very small amounts. In Sec. 4.6, we showed that observations constrain σ_k to be between 0.0 and 0.1. By adopting $\sigma_k = 0.1$, we obtained the brightest $M_V(RR)$ consistent with this constraint; adopting a smaller value of σ_k results in values of $M_V(RR)$ up to 0.03 mag *fainter*. Had we corrected for the small bias uncovered by our halo simulations (Sec. 4.8), our result would have been ∼0.04 mag *brighter*. Had we retained the 3 velocity dispersion covariance parameters in our model (Sec. 4.7), our result would have been 0.02 mag *brighter*. Had we adopted the sample Halo-2 rather than Halo-3, our result would have been ∼0.01 mag *fainter*.

A final note in favor of our $M_V(RR)$ zero-point comes from the derived kinematics (e.g., Sec. 3). If the brighter Sandage (1993) $M_V(RR)$ is used, the velocity dispersions for the local thick disk and halo grow by 5-10%. The dispersions derived from our stat-π solutions and presented in Table 6 are in good agreement with estimates of the velocity ellipsoids of these components as measured by other tracers (in fact, the σ_U value for the halo is already larger than many estimates). Enlarging them to match the brighter $M_V(RR)$ degrades this agreement.

7. Consequences for Distances And Ages

As discussed in Sec. 1, the $M_V(RR)$–[Fe/H] relation, in particular its zero-point, is important in determining a number of quantities of interest to both Galactic and extra-galactic astronomy. In this section, we present the implications of our stat-π–derived $M_V(RR)$ zero-point.

In Sec. 5.4, we were unable to obtain a meaningful value for the slope of the $M_V(RR)$–[Fe/H] relation. However, our zero-point for the halo RR Lyraes is quite well determined. In the following discussion, we adopt our zero-point along with a slope $\Delta M_V(RR)/\Delta[\mathrm{Fe/H}] = 0.15$ mag dex^{-1}, in agreement with HB theory (Lee 1990), RGB theory (Fusi Pecci *et al.* 1990), Baade-Wesselink observations (Jones *et al.* 1992), and some analyses of the Sandage period shift effect (CSJ, Fernley 1993). Specifically, we adopt the relation $M_V(RR) = 0.15[\mathrm{Fe/H}] + 0.95$ mag.

7.1. Distance to the Galactic Center

Walker & Mack (1986) obtained the distance to the Galactic Center, R_0, by finding the peak in the space density of RR Lyraes as a function of distance along the line of sight through Baade's Window (BW). They recalibrated the photographic photometry of Blanco (1984) to the Johnson B band using several CCD standard fields, corrected it for interstellar absorption, and converted it to the V band using a $\langle B\rangle_0 - \langle V\rangle_0$ *vs.* Period relation obtained from NGC 6171. They found $R_0 = 8.1 \pm 0.4$ if $M_V(RR) = +0.60$ mag.

We repeat their analysis here, comparing the results obtained using both their preferred value of $M_V(RR) = +0.60$ mag, and our preferred value of $M_V(RR) = 0.15[\mathrm{Fe/H}] + 0.95$ mag. We employ the newer reddening estimates of $E(B-V) = 0.50$ for BW (Walker & Terndrup 1991) and $E(B-V) = 0.33$ for NGC 6171 (Harris 1994). We also employ the Walker & Terndrup (1991) ΔS metallicities, rather than the photometric ones used by Walker & Mack (1986). Like those authors, we found that a small shift (+0.04 mag) should be applied to make the fitted line in the $\langle B\rangle_0 - \langle V\rangle_0$ *vs.* Period plane coincide with the BW RR Lyraes listed in their Table 7, presumably to correct for slight inconsistencies in the adopted reddenings and/or metallicities of the cluster RR Lyraes relative to those in BW.

Figure 8 shows the space density of stars (in arbitrary units) as a function of distance through BW. Using a variety of methods, we find that the curve based on $M_V(RR) = 0.15[\mathrm{Fe/H}] + 0.95$ peaks at $R = 7.4$ kpc (squares), while that based on $M_V(RR) = +0.60$ peaks at $R = 8.1$ kpc (circles). After applying the small geometric correction of 1.03 discussed by Walker & Mack (1986), we obtain $R_0 = 7.6 \pm 0.4$ and $R_0 = 8.3 \pm 0.5$, respectively.

We note that the relation $M_V(RR) = 0.15[\mathrm{Fe/H}] + 0.725$ mag, based on the Walker (1992) zero-point (see Table 7) produces results almost identical with those of the $M_V(RR) = +0.60$ relation. We also note that the widths of the density curves produced using these three $M_V(RR)$–[Fe/H] relations are nearly identical, after they are corrected for the distance scale effects produced by the

different distance zero-points. This supports the statement by Walker & Terndrup (1991) that the abundance dispersion in BW is too small to meaningfully constrain the slope of the $M_V(RR)$–[Fe/H] relation using this method.

The short distance to the Galactic Center based on our stat-π zero-point is favored by the "primary" distance source, H_2O maser proper motions ($R_0 = 7.2 \pm 1.3$ kpc), quoted by Reid (1993). Reid lists a number of other R_0 estimates, and from them derives a "best value" of $R_0 = 8.0 \pm 0.5$ kpc. As noted by Carney *et al.* (1995), this value is in part determined using a "bright" RR Lyrae calibration. If we recompute the "best value" excluding the optical RR Lyrae-dependent methods, we obtain $R_0 = 7.9 \pm 0.6$ kpc. This value is further supported by Carney *et al.* (1995), who recently found $R_0 = 7.8 \pm 0.4$ kpc from the K-band photometry of 58 RR Lyrae stars in BW, as calibrated using the $M_K(RR)$–log($Period$) relation of CSJ.

7.2. Ages of Globular Clusters

The age of a globular cluster can be determined by comparing the absolute magnitude of its main-sequence turnoff (MSTO) with the MSTOs of theoretical isochrones. The difference in apparent magnitude between a cluster's RR Lyraes and its MSTO, together with an adopted value for $M_V(RR)$, can be used to find the absolute magnitude of the cluster's MSTO.

It is instructive to see the difference between the ages derived using our $M_V(RR)$ zero-point and those using the brighter zero-point of Walker (1992). For both cases, we adopt a metallicity dependence of 0.15 mag dex^{-1}, so the relations are $M_V(RR) = 0.15$ [Fe/H] + 0.95, and $M_V(RR) = 0.15$ [Fe/H] + 0.725, respectively. The zero-point of the $M_V(RR)$–[Fe/H] relation primarily determines the mean age of the globular cluster system, while the slope of the relation determines the age distribution. Thus our comparison focuses on the mean ages of the halo globular cluster system under the two $M_V(RR)$ zero-points.

Brian Chaboyer has kindly computed ages for the 39 "older" clusters listed in Table 3 of Chaboyer, Demarque & Sarajedini (1996b) using both of these $M_V(RR)$–[Fe/H] relations. The ages were derived using the OPAL equation of state isochrones of Chaboyer & Kim (1995). These isochrones include the effects of diffusion and the latest available equation of state (Rogers 1994), and employ modern helium and α-element abundances.

The weighted mean age of the 39 clusters is 14.8 ± 0.2 Gyr using our zero-point, and 11.7 ± 0.2 Gyr using the Walker (1992) zero-point (standard errors of the mean). We account for the uncertainties in the $M_V(RR)$ zero-points by computing the mean ages from $M_V(RR)$–[Fe/H] relations based on zero-points of $M_V(RR) \pm \sigma_{Mv}$ (again, thanks to B. Chaboyer). For our stat-π $M_V(RR)$ zero-point, the mean age including formal errors is $14.8^{+2.1}_{-1.8}$ Gyr, compared with $11.7^{+1.4}_{-1.3}$ Gyr using the Walker (1992) zero-point. These values are $\sim$14% smaller than the ages computed without the improved treatments of diffusion and the equation of state (Chaboyer *et al.* 1996b). Clearly, the $M_V(RR)$ zero-point derived from the present stat-π analysis supports an older age for the globular

cluster system.

The ages of the *oldest* globular clusters place a lower limit on the age of the Universe. Chaboyer *et al.* (1996a) define a group of 17 clusters which they suspect represents the oldest Galactic globulars. Using the method described above, their weighted mean age is $16.5^{+2.1}_{-1.9}$ Gyr using our stat-π $M_V(RR)$ zero-point, and $13.1^{+1.5}_{-1.3}$ Gyr using Walker's zero-point. A word of caution is warranted here. The median [Fe/H] of this group is $\sim$0.2 dex lower than that of the field RR Lyraes used to determine the $M_V(RR)$ zero-point, so if the $M_V(RR)$–[Fe/H] slope is 0.30 (0.0) mag dex^{-1}, the mean derived ages are $\sim$ 0.5 Gyr smaller (larger) than those quoted.

7.3. Distance to the LMC and its Effect on H_0

Walker (1992) lists the de-reddened $\langle V \rangle_I$ magnitudes of the RR Lyrae stars in seven Large Magellanic Cloud (LMC) globular clusters. Using an LMC distance modulus of 18.50 $\pm$ 0.10, based on LMC Cepheid observations and an abundance-corrected Galactic Cepheid calibration, he obtained $M_V(RR) = +0.44$ at [Fe/H] = –1.9, consistent with the "brighter" $M_V(RR)$ values shown in Fig. 7. This distance modulus implies an LMC distance of 50 ± 2 kpc.

Using Walker's $\langle V \rangle_I$ magnitudes, and adopting $M_V(RR)$ = 0.15[Fe/H] + 0.95, based on our new stat-π zero-point, we find the LMC distance modulus to be 18.28 $\pm$ 0.13, equivalent to a distance of 45 $\pm$ 3 kpc.

Given the complexities of deriving the Cepheid period-luminosity relation (see Sec. 6, also Walker (1992) and references therein), it seems worthwhile to explore the consequences of applying a zero-point offset to the Cepheid period-luminosity relation to make it match the shorter LMC distance based on our stat-π results.

A particularly interesting consequence involves the measurement of the Hubble constant, H_0. Many extra-galactic distance indicators are calibrated to, or are consistent with, an LMC distance modulus of 18.50 mag. If the distances determined using these indicators are recalibrated to agree with our smaller LMC distance modulus, the value of H_0 derived from them increases by 10%. For example, the recent Cepheid-based distance of 15.8 ± 1.3 Mpc to M100 yielded $H_0 = 83 \pm 16$ km s^{-1} Mpc^{-1} (Ferrarese *et al.* 1996). If we reduce the M100 distance modulus by 0.22 mag to bring the Cepheid period-luminosity relation into agreement with our LMC distance, we obtain $d_{M100} = 14.3 \pm 1.2$ Mpc and $H_0 = 92 \pm 18$ km s^{-1} Mpc^{-1}.

Freedman *et al.* (1994; their Fig. 3) have already shown that the expansion age of the Universe implied by $H_0 = 80 \pm 17$ km s^{-1} Mpc^{-1} in the framework of the Einstein–de Sitter cosmological model is in conflict with the observed ages of globular clusters. Our stat-π $M_V(RR)$ zero-point indicates a larger value of H_0 (shorter expansion time) and older globular clusters, thus increasing the disagreement between these two important observables. The disagreement persists even at lower values of the density parameter ($\Omega \approx 0.1$). However, other recent measurements of H_0 obtain

lower values which are in better agreement with our cluster ages. For example, Branch *et al.* (1996) obtained $H_0 = 57 \pm 4$ km s^{-1} Mpc^{-1} from Type Ia supernovae.

Additional possible routes to reconciling observations of H_0 and globular cluster ages include accepting a non-zero cosmological constant (Carroll & Press 1992) and further refinements to stellar evolution theory which result in younger cluster ages (e.g., Mazzitelli *et al.* 1995).

8. Conclusions

We have assembled high-quality data on 213 nearby RR Lyrae variables. These data include new absolute proper motions from the Lick Northern Proper Motion program (Klemola *et al.* 1993) and abundances and radial velocities from Layden (1994). Based on an *a priori* kinematic study, we defined three ways to separate the stars into thick disk and halo sub-populations. Statistical parallax solutions for these sub-samples yielded the absolute magnitude and kinematics of the RR Lyraes in the samples. We note that our $M_V(RR)$ values correspond to the absolute magnitude of typically-evolved RR Lyrae stars, not to that of the Zero Age Horizontal Branch.

For the halo population, the solutions produced a well determined absolute magnitude, $M_V(RR) = +0.71 \pm 0.12$ at $\langle[\mathrm{Fe/H}]\rangle = -1.61$. The derived kinematics, $\langle V\rangle = -210 \pm 12$ km s^{-1} and $(\sigma_U, \sigma_V, \sigma_W) = (168 \pm 13,\ 102 \pm 8,\ 97 \pm 7)$ km s^{-1}, are in good agreement with previous estimates of the halo RR Lyrae kinematics, and with the kinematics of other stellar tracers of the halo.

For the thick disk population, the results of the three definitions scatter somewhat, and the uncertainties are larger. Our best estimate for the thick disk was $M_V(RR) = +0.79 \pm 0.30$ at $\langle[\mathrm{Fe/H}]\rangle = -0.76$, after correction for the bias mentioned below. The derived kinematics, $\langle V\rangle = -48 \pm 9$ km s^{-1} and $(\sigma_U, \sigma_V, \sigma_W) = (56 \pm 8,\ 51 \pm 8,\ 31 \pm 5)$ km s^{-1}, again are in good agreement with previous estimates of the thick disk kinematics based on RR Lyraes and on other tracers.

The large uncertainty in the disk solution prevented us from deriving a meaningful slope for the $M_V(RR)$–[Fe/H] relation. An attempt to measure the slope by sub-dividing the halo sample into two metallicity bins also failed to meaningfully determine the slope.

Monte Carlo tests using simulated data showed that our stat-π code accurately returns the true kinematic and M_V values of the input data. They also revealed the possibility that the internal errors returned by the HJBW stat-π algorithm may be overestimates. For the halo, the true error of $M_V(RR)$ may be $\sim$0.08 mag rather than 0.12 mag. The kinematic results for both the disk and halo may also be more precise than the errors cited above. However, it is outside the scope of this paper to determine which set of error values is correct. So, for the present, we have conservatively adopted the larger values.

The simulations also enabled us to evaluate the effects of other factors on the solutions. All were negligible, except for a small bias towards "short" distance scales that is observed when the U and V velocity dispersions are of comparable size. We determined corrections based on the

simulations: –0.15 mag for the disk and –0.04 mag for the halo solutions. The former correction was applied to the real-data solutions, while the latter was deemed too small to be of practical value.

We discussed the effects of systematic errors. The main systematic uncertainty is in the adopted reddening scale. Our scale (Burstein & Heiles 1982) makes our $M_V(RR)$ value $\sim$0.11 mag fainter than it would have been using the Sturch (1966) reddenings, but SRM argue that the former scale is preferred. Our adopted photometric scale makes our quoted $M_V(RR)$ value as bright as possible ($\sim$0.07 mag). Several other minor systematics, including the halo bias correction noted above, were also considered. It is unlikely that these systematic errors alone can account for the difference between our $M_V(RR)$ value and the brighter ($\sim$0.2 mag) values found by some authors (e.g., Buonanno *et al.* 1990; Sandage 1990b, 1993; Walker 1992).

Unlike the methods used by many authors, the stat-π method is independent of other distance calibrations. It also depends on a relatively simple and well-tested model (Galactic kinematics) in comparison to the other methods, which employ model atmospheres, stellar evolution theory, empirical color–temperature relations, RR Lyrae mass determinations, etc.

We investigated the implications of our halo $M_V(RR)$ by using an $M_V(RR)$–[Fe/H] relation based on an adopted slope of $\Delta M_V/\Delta[\mathrm{Fe/H}] = 0.15$ mag dex^{-1} in combination with our halo zero-point. We found the distance to the Galactic Center to be $R_0 = 7.6 \pm 0.4$ kpc based on observations of the RR Lyraes in Baade's Window, in good agreement with many other estimates of R_0. Using the "brighter" $M_V(RR)$ values, R_0 is 10% larger. Following Chaboyer *et al.* (1996b), we found the mean age of the 17 oldest Galactic globular clusters to be $16.5^{+1.9}_{-2.1}$ Gyr, 3.4 Gyr older than the mean age obtained using the brighter RR Lyrae zero-point; this places an important lower limit on the age of the Universe. We found the distance modulus of the Large Magellanic Cloud to be 18.28 ± 0.13 mag. Any estimates of the Hubble Constant, H_0, which are based on an LMC distance modulus of 18.50 mag (e.g., the Cepheid study of Ferrarese *et al.* 1996) increase by 10% if their distance scales are recalibrated to match our LMC distance. This increase implies a younger age for the Universe, in conflict with the older globular cluster ages derived from our $M_V(RR)$ value. The conflict is lessened or eliminated if the true value of H_0 is low, if the cosmological constant is non-zero, or if further refinements to stellar evolution theory result in younger cluster ages.

The authors acknowledge valuable discussions with Drs. Brian Chaboyer, Jan Lub, Robert Schommer, and Alistair Walker. The comments of an anonymous referee improved several sections of the paper. ACL acknowledges financial support from the Natural Sciences and Engineering Research Council of Canada, through research grants to W.E. Harris and D.L. Welch, and from Cerro Tololo Inter-American Observatory. The Lick Northern Proper Motion program is supported by National Science Foundation grant AST 92-18084. SLH acknowledges the support of NSF Young Investigator (NYI) grant number AST94-57455. CJH performed part of this research as an REU student at Michigan State University.

REFERENCES

Ajhar, E.A., Grillmair, C.J., Lauer, T.R., Baum, W.A., Faber, S.M., Holtzman, J.A., Lynds, C.R. & O'Neil, E.J.Jr. 1996, AJ, 111, 1110

Barnes III, T.G., & Hawley, S.L. 1986, ApJ, 307, L9 (BH86)

Beers, T.C. 1996, Formation of the Galactic Halo ... Inside and Out, ASP Conf. Ser. 92, eds. H. Morrison & A. Sarajedini, (ASP: San Francisco), 130

Blanco, B.M. 1984, AJ, 89, 1836

Blanco, V.M. 1992, AJ, 104, 734

Bolte, M. & Hogan 1995, Nature, 376, 399

Bookmyer, B.B., Fitch, W.S., Lee, T.A., Wisniewski, W.Z. & Johnson, H.L. 1977, Rev. Mex. Astron. Astrofis., 2, 235

Branch, D., Romanishin, W., & Baron, E. 1996, ApJ, 465, 73

Buonanno, R., Corsi, C.E. & Fusi Pecci, F. 1989, A&A, 216, 80

Buonanno, R., Cacciari, C., Corsi, C.E. & Fusi Pecci, F. 1990, A&A, 230, 315

Burstein, D., & Heiles, C. 1982, AJ, 87, 1165

Carney, B.W., Storm, J. & Jones, R.V. 1992, ApJ, 386, 663 (CSJ)

Carney, B.W., Fulbright, J.P., Terndrup, D.M., Suntzeff, N.B., & Walker, A.R. 1995, AJ, 110, 1674

Carrol, S.M. & Press, W.H. 1992, ARA&A, 30, 499

Casertano, S., Ratnatunga, K.U., & Bahcall, J.N. 1990, ApJ, 357, 435

Chaboyer, B. 1995, ApJ, 444, L9

Chaboyer, B. & Kim, Y.-C. 1995, ApJ, 454, 767

Chaboyer, B., Demarque, P., Kerman, P.J. & Krauss, L.M. 1996a, Science, 271, 957

Chaboyer, B., Demarque, P. & Sarajedini, A. 1996b, ApJ, 459, 558

Clube, S.V.M. & Dawe, J.A. 1980a, MNRAS, 190, 575

Clube, S.V.M. & Dawe, J.A. 1980b, MNRAS, 190, 591 (CD80)

Croswell, K., Latham, D.W. & Carney, B.W. 1987, AJ, 93, 1445

Eggen, O.J., Lynden-Bell, D. & Sandage, A. 1962, ApJ, 136, 748

Fernley, J. 1993, A&A, 268, 591

Ferrarese, L., *et al.* 1996, ApJ, 464, 568

Fitch, W.S., Wisniewski, W.Z. & Johnson, H.L. 1966, Comm. Lunar Planet. Lab., No. 71, 3

FitzGerald, M.P. 1968, AJ, 73, 983

FitzGerald, M.P. 1987, MNRAS, 229, 227

Freedman, W.L., *et al.* 1994, Nature, 371, 757

Fusi Pecci, F., Ferraro, F.R., Crocker, D.A., Rood, R.T. & Buonanno, R. 1990, A&A, 238, 95

Gould, A. 1995, ApJ, 452, 189

Harris, W.E. 1994 http://www.physics.mcmaster.ca/Globular.html

Hanson, R.B. 1993, Lick Northern Proper Motion Program: NPM1 Catalog – Documentation for the Computer-Readable Version, National Space Science Data Center Document No. NSSDC/WDC-A-R&S 93-41

Hanson, R.B., & Klemola, A.R. 1994, Lick Northern Proper Motion Program: NPM1 Catalog Cross-Identifications and Appendices – Documentation for the Computer-Readable Version, National Space Science Data Center Document No. NSSDC/WDC-A-R&S 94-14

Hawley, S.L., Jefferys, W.H., Barnes III, T.G. & Wan, L. 1986, ApJ, 302, 626 (HJBW)

Hemenway, M.K. 1975, AJ, 80, 199

Johnson, D.R.H. & Soderblom, D.R. 1987, AJ, 93, 864

Jones, R.V., Carney, B.W., & Latham, D.W. 1988, ApJ, 332, 206

Jones, R.V., Carney, B.W., Storm, J. & Latham, D.W. 1992, ApJ, 386, 646

Joy, A.H. 1950, PASP, 62, 60

Jurcsik, J. & Kovács, G. 1996, A&A, in press

Kerr, F.J. & Lynden-Bell, D. 1986, MNRAS, 221, 1023

Kholopov, P.N. 1985, General Catalog of Variable Stars, 4th Ed., (Nauka, Moscow)

Klemola, A.R., Hanson, R.B. & Jones, B.F. 1993, Lick Northern Proper Motion Program: NPM1 Catalog, National Space Science Data Center – Astronomical Data Center Catalog No. A1199

Klemola, A.R., Hanson, R.B. & Jones, B.F. 1994a, Lick Northern Proper Motion Program: NPM1 Catalog Cross-Identifications and Appendices, National Space Science Data Center – Astronomical Data Center Catalog No. A1214

Klemola, A.R., Hanson, R.B. & Jones, B.F. 1994b, Lick NPM Program: NPM1 Catalog and its Applications, in Galactic and Solar System Optical Astrometry, eds. L.V. Morrison and G.F. Gilmore, Cambridge, Cambridge University Press, pp. 20-25

Klemola, A.R., Jones, B.F. & Hanson, R.B. 1987, AJ, 94, 501

Lambert, D.L., Heath, J.E., Lemke, M., & Drake, J. 1995, ApJS, 104, 183

Landolt, A.U. 1992, AJ, 104, 340

Layden, A.C. 1994, AJ, 108, 1016 (L94)

Layden, A.C. 1995, AJ, 110, 2288 (L95)

Layden, A.C., Hawley, S.L. & Hanson, R.B. 1994, BAAS, 184, 3202

Layden, A.C., 1996, in preparation

Lee, Y.-W., Demarque, P. & Zinn, R. 1990, ApJ, 350, 155

Lee, Y.-W. 1990, ApJ, 363, 159

Lub, J., 1977, Ph.D. dissertation, Leiden University

Lutz, T.E. & Hanson, R.B. 1992, ASP Conf. Series, 25, 257

Majewski, S.R. 1993, ARA&A, 31, 575

Mazzitelli, I., D'Antona, F. & Caloi, V. 1995, A&A, 302, 382

Mihalas, D. & Binney, J. 1981, Galactic Astronomy, Second Edition, (Freedman: San Francisco)

Morrison, H.L., Flynn, C. & Freeman, K.C. 1990, AJ, 100, 1191

Nissen, P.E. & Schuster, W.J. 1991, A&A, 251, 457

Murray, C.A. 1983, Vectorial Astrometry, Bristol, Adam Hilger Ltd., pp. 297-302

Pel, J.W., 1976, A&A Supp, 24, 413

Pierce, M.J., Welch, D.L., McClure, R.D., van den Bergh, S., Racine, R., & Stetson, P.B. 1994, Nature, 371, 385

Preston, G.W. 1959, ApJ, 130, 507

Reid, M.J. 1993, ARA&A, 31, 345

Rogers, F.J. 1994, in The Equation of State in Astropyhsics, IAU Coll. 147, ed. G. Chabrier and E. Schatzman (Cambridge: Cambridge University Press), 16

Sandage, A. 1990a, ApJ, 350, 603

Sandage, A. 1990b, ApJ, 350, 631

Sandage, A. 1993, AJ, 106, 703

Schmidt, E.G. 1991, AJ, 102, 1766

Schmidt, E.G., Chab, J.R., Reiswig, D.E. 1995, AJ, 109, 1239

Searle, L. & Zinn, R. 1978, ApJ, 225, 357

Strugnell, P., Reid, N. & Murray, C.A. 1986, MNRAS, 220, 413 (SRM)

Sturch, C.R. (1966), ApJ, 143, 774

Walker, A.R. 1992, ApJ, 390, L81

Walker, A.R. & Mack, P. 1986, MNRAS, 220, 69

Walker, A.R. & Terndrup, D.M. 1991, ApJ, 378, 119

Wan, L., He, M.-F., Zhu, G.-L., & Li, Z.-Y. 1979, Chinese Astronomy, 3, 296

Wan, L., Mao, Y.-Q. & Ji, D.-S. 1980, Ann. Shanghai Obs., No. 2, 1 (WMJ)

Yi, S., Lee, Y.-W. & Demarque, P. 1993, ApJ, 411, L25

Zinn, R.J. 1993, The Globular Cluster–Galaxy Connection, ASP Conf. Ser. 48, eds. G.H. Smith & J.P. Brodie, (ASP: San Francisco), 38

Zinn, R., & West, M.J. 1984, ApJS, 55, 45

Figure Captions

Fig. 1.— The difference in proper motions measured by the Lick NPM program and listed in the WMJ compilation (in the sense NPM–WMJ) is plotted as a function of the proper motion error given by WMJ, for (a) the right ascension component, and (b) the declination component. In each panel, the solid horizontal line represents the mean proper motion difference for all stars plotted: $-0\farcs11 \pm 0\farcs09$ cent^{-1} in $\Delta\mu_\alpha$ (105 stars) and $-0\farcs18 \pm 0\farcs08$ cent^{-1} in $\Delta\mu_\delta$ (107 stars).

Fig. 2.— The running values of the nominal total RMS error (labeled "tot") and of the actual RMS dispersion of the proper motion differences (labeled "$\Delta\mu$") are plotted as a function of the "rank" of the WMJ proper motion error (rank 1 = smallest), for (a) the right ascension component, and (b) the declination component. In each panel, the short-dashed horizontal line ("NPM") represents the fixed contribution of the NPM proper motion error $0\farcs5$ cent^{-1}, and the long-dashed line shows a constant RMS error ($0\farcs85$ cent^{-1} in $\Delta\mu_\alpha$; $0\farcs80$ cent^{-1} in $\Delta\mu_\delta$). See Sec. 2.1 for further explanation.

Fig. 3.— The (a) radial, and (b) vertical components of space velocity are plotted as a function of rotational velocity for 213 RR Lyraes. Squares indicate NPM proper motions, while triangles indicate proper motions from WMJ. Solid symbols have [Fe/H] > -1, while open symbols have [Fe/H] ≤ -1.

Fig. 4.— The rotational component of space velocity is plotted as a function of abundance for 213 RR Lyraes. Squares and triangles indicate NPM and WMJ proper motions, respectively. The sloping line separates disk and halo stars according to Definition 1 (see Table 3), while the dash-dot line indicates the separation according to Definition 2. Filled symbols indicate stars belonging to the disk, according to Definition 3, while open symbols indicate stars belonging to the halo. The vertical dotted line separates the groups Halo-1P and Halo-1R.

Fig. 5.— Monte Carlo simulation results for 18 disk data sets (filled squares) and 20 halo data sets (open squares), listed respectively as solutions D2d and H2d in Table 5. The difference between the absolute magnitude computed using the stat-π method and that "built into" the data set is plotted as a function of the velocity dispersion ratio σ_U/σ_V (see Sec. 4.8). The solid line is the

This preprint was prepared with the AAS LaTeX macros v4.0.

least-squares fit to the disk solutions, and the dashed line marks the mean of the halo solutions. The arrows mark the velocity dispersion ratios of the real data (Disk-3 and Halo-3).

Fig. 6.— The stat-π solutions for the real star sub-samples listed in Table 6 are plotted in the abundance–magnitude plane. Circles mark the solutions for the Disk-1 and Halo-1 sub-samples, squares mark the Disk-2 and Halo-2 solutions, and triangles mark the Disk-3 and Halo-3 solutions. Filled symbols indicate results after correction for the σ_U/σ_V bias discussed in Sec. 4.8, while open symbols (dotted error bars) indicate pre-correction solutions. The crosses mark the solutions for Halo-1P and Halo-1R.

Fig. 7.— Our final stat-π solutions for $M_V(RR)$ are plotted against abundance (circles), together with the results of other $M_V(RR)$ studies. The symbol keys are given in the right-most column of Table 7.

Fig. 8.— The space density of RR Lyraes (in arbitrary units) as a function of distance along the line of sight through Baade's Window. Squares mark the distribution which employed $M_V(RR) = 0.15[\mathrm{Fe/H}] + 0.95$, while circles mark the distribution obtained using $M_V(RR) = +0.60$ mag. The dotted lines present an alternate binning scheme for the two distributions.

Table 1. RR Lyrae Photometry Correlations.

Source[a]	$\langle V \rangle_{I,CD80}$	Std Dev	N_{stars}
1	$0.146 + 0.983 \cdot \langle V \rangle_{I,B77}$	0.050	42
2	$6.873 + 0.985 \cdot 2.5 \cdot \langle V \rangle_L - 0.034 \cdot 2.5 \cdot \langle V - B \rangle_L$	0.054	51
3	$-0.086 + \langle V \rangle_{I,S}$	0.064	13

[a]Sources: 1=Bookmyer *et al.* 1977; 2=Lub 1977; 3=Schmidt *et al.* 1991, 1995.

Table 2. Basic Data.

Star	NPM1	l	b	μ_α	μ_δ	V_{rad}	ϵ_V	[Fe/H]	$\langle V\rangle_I$	A_V	Ref	D/
		°	°	″/cent	″/cent	km/s	km/s	dex	mag	mag	[a]	
SW And	+29.0017	115.72	–33.09	0.53	–2.49	–21	2	–0.38	9.68	0.14	1121	11
XX And	+38.0072	128.45	–23.64	3.53	–3.56	0	5	–2.01	10.63	0.13	1111	00
XY And	+33.0068	131.22	–28.23	1.34	–0.28	–64	53	–0.92	13.63	0.15	1161	00
ZZ And	+26.0036	122.42	–35.85	2.50	–1.80	–13	53	–1.58	13.01	0.12	1141	00
CI And	+43.0105	134.93	–17.62	–0.15	–0.38	99	30	–0.83	12.15	0.26	1141	11
DR And	+33.0052	126.16	–28.57	3.00	–1.38	–81	30	–1.48	12.34	0.09	1141	00
WY Ant	–	266.93	22.08	2.56	–4.81	211	24	–1.66	10.83	0.18	2111	00
SW Aqr	–00.1628	51.31	–31.47	–4.67	–6.08	–42	8	–1.24	11.14	0.22	1111	00
SX Aqr	+03.1345	57.90	–34.00	–3.87	–5.14	–166	7	–1.83	11.70	0.11	1111	00
TZ Aqr	–05.1879	53.25	–44.33	0.96	–1.77	–35	12	–1.24	12.01	0.10	1121	00
YZ Aqr	–11.1939	48.93	–49.76	–1.25	0.21	–150	14	–1.55	12.65	0.08	1161	00
AA Aqr	–10.2266	54.63	–53.83	2.11	–0.30	–20	14	–2.09	12.37	0.15	1161	00
BN Aqr	–07.2815	56.22	–50.73	0.96	–3.26	–182	30	–1.33	12.52	0.10	1161	00
BO Aqr	–12.2527	55.40	–58.83	–0.82	–1.21	–24	13	–1.80	12.11	0.07	1111	00
BR Aqr	–09.2377	75.48	–65.24	0.50	–0.02	29	10	–0.84	11.40	0.04	1121	11
BT Aqr	–05.1748	42.94	–30.60	–0.30	–1.06	–52	11	–0.29	12.34	0.12	1121	11
CP Aqr	–01.1098	48.74	–31.34	–1.45	–1.73	29	21	–0.90	11.71	0.11	1131	11
DN Aqr	–	35.76	–69.06	4.60	–1.60	–214	8	–1.63	11.18	0.02	2131	00
AA Aql	–03.1592	43.08	–24.99	–1.80	–1.54	–32	4	–0.58	11.74	0.21	1121	11
V341 Aql	–	45.62	–22.04	3.48	–2.40	–81	4	–1.37	10.81	0.31	2121	00
X Ari	+10.0299	169.08	–39.84	5.97	–9.24	–35	3	–2.40	9.51	0.50	1111	00
TZ Aur	+40.0228	176.79	20.92	–0.30	–1.35	46	6	–0.80	11.86	0.18	1121	11
RS Boo	+31.0704	50.84	67.35	0.22	–1.17	–9	2	–0.32	10.36	0.00	1121	11
ST Boo	+35.0720	57.39	55.22	–1.54	–1.67	13	4	–1.86	10.98	0.04	1121	00
SV Boo	+39.0683	68.75	65.51	–0.17	–2.28	–131	22	–1.55	13.12	0.00	1121	00
SW Boo	+36.0643	62.52	67.74	–4.58	0.13	–18	18	–1.12	12.34	0.00	1111	00
SZ Boo	+28.0840	41.93	65.50	–0.77	–0.85	–38	21	–1.68	12.60	0.01	1111	00
TW Boo	+41.0778	71.06	62.85	0.34	–5.86	–99	4	–1.41	11.20	0.01	1121	00
UU Boo	+35.0710	56.50	58.01	0.86	–3.38	10	28	–1.92	12.22	0.01	1121	00
UY Boo	+13.0991	354.24	68.81	–0.28	–4.51	144	3	–2.49	10.80	0.00	1121	00
RZ Cam	+67.0052	147.98	23.17	0.75	–0.57	–266	26	–1.01	12.73	0.18	1121	00
RW Cnc	+29.0370	197.49	43.53	0.79	–4.17	–85	7	–1.52	11.85	0.03	1161	00
SS Cnc	+23.0300	198.94	26.28	–0.77	–1.72	–27	16	–0.07	12.16	0.09	1121	11
TT Cnc	+13.0361	212.10	28.38	–4.60	–4.00	49	5	–1.58	11.24	0.12	1111	00
AN Cnc	+15.0560	212.10	35.03	–0.51	–2.53	16	14	–1.45	13.16	0.06	1141	00
AQ Cnc	+12.0610	218.04	38.10	–1.15	–3.39	390	20	–1.53	12.00	0.04	1141	00

Table 2—Continued

Star	NPM1	l	b	μ_α	μ_δ	V_{rad}	ϵ_V	[Fe/H]	$\langle V\rangle_I$	A_V	Ref	D
		$\circ$	$\circ$	″/cent	″/cent	km/s	km/s	dex	mag	mag	[a]	
AS Cnc	+25.0305	197.89	31.23	2.79	–0.83	258	26	–1.89	12.50	0.05	1141	00
W CVn	+38.0637	71.82	70.96	–1.71	–0.89	18	21	–1.21	10.52	0.00	1111	00
Z CVn	+44.0884	124.00	73.35	–0.79	–3.97	14	10	–1.98	11.93	0.00	1121	00
RR CVn	+34.0596	154.05	81.09	–1.58	–3.17	–5	21	–1.08	12.55	0.01	1111	00
RU CVn	+31.0668	53.96	74.51	–2.97	0.22	–27	21	–1.37	11.96	0.00	1121	00
RX CVn	+41.0711	87.08	71.53	–0.20	0.10	–158	28	–1.31	12.57	0.00	1121	00
RZ CVn	+32.1089	61.59	77.15	–5.84	–0.36	–12	7	–1.92	11.42	0.00	1121	00
SS CVn	+40.0608	83.85	72.63	1.24	–5.10	–15	22	–1.52	11.89	0.00	1121	00
SV CVn	+37.0978	139.98	79.40	0.12	–2.55	29	28	–2.20	12.59	0.00	1121	00
SW CVn	+37.0987	134.84	79.80	–0.96	–1.98	–18	21	–1.53	12.74	0.00	1121	00
UZ CVn	+40.0532	139.53	75.93	0.06	–2.32	–38	26	–2.34	12.02	0.00	1141	00
AL CMi	+05.0339	214.43	15.35	–1.21	–0.52	46	21	–0.85	12.01	0.09	1151	1
RV Cap	–15.2350	33.13	–35.54	2.42	–10.57	–106	7	–1.72	10.92	0.11	1111	00
IU Car	–	269.59	–22.95	–1.30	0.60	328	18	–1.85	11.91	0.39	2111	00
V499 Cen	–	315.10	18.12	2.10	–0.25	323	24	–1.56	11.05	0.18	2111	00
DX Cep	+83.0238	119.50	21.95	1.86	0.91	–6	30	–1.83	12.67	0.35	1161	00
RR Cet	+01.0121	143.54	–59.89	–0.05	–3.88	–75	1	–1.52	9.75	0.02	1111	00
RU Cet	–16.0129	134.27	–78.63	2.15	–1.00	57	8	–1.60	11.60	0.01	1111	00
RV Cet	–11.0305	177.32	–64.40	2.58	–1.83	–93	7	–1.32	10.76	0.02	1111	00
RX Cet	–15.0060	102.48	–77.64	–2.89	–6.25	–58	7	–1.46	11.36	0.03	1111	00
RZ Cet	–08.0299	178.21	–60.34	2.59	1.88	–10	6	–1.50	11.84	0.03	1121	00
XZ Cet	–16.0267	182.40	–70.75	4.14	–0.13	167	10	–2.27	9.49	0.00	1161	00
RY Col	–	246.47	–35.05	3.60	1.80	482	15	–1.11	10.86	0.01	2131	00
S Com	+27.0979	213.16	85.84	–2.22	–2.01	–55	4	–2.00	11.55	0.02	1111	00
V Com	+27.0931	208.67	80.85	–0.84	0.47	23	28	–1.75	13.16	0.02	1121	00
RY Com	+23.0619	342.56	85.06	–0.61	–1.78	–31	8	–1.65	12.30	0.04	1121	00
TV CrB	+27.1359	41.33	56.51	–0.31	–1.01	–157	48	–2.33	11.61	0.07	1161	00
W Crt	–17.1378	276.00	40.47	–2.38	–1.48	65	13	–0.50	11.51	0.09	1121	1
X Crt	–10.1333	278.87	49.49	–0.13	–3.55	79	4	–1.75	11.48	0.00	1111	00
XZ Cyg	–	88.21	16.98	8.43	–2.15	–119	14	–1.52	9.72	0.33	2111	00
DM Cyg	+31.0966	79.46	–12.41	1.34	–0.72	12	23	–0.14	11.49	0.69	1121	1
DX Del	+12.1761	58.47	–18.84	1.41	–1.17	–45	3	–0.56	9.92	0.32	1121	1
RW Dra	+57.0740	87.39	40.60	–0.23	–0.82	–108	22	–1.40	11.57	0.00	1121	00
SU Dra	+67.0274	133.44	48.27	–4.95	–7.26	–167	1	–1.74	9.78	0.00	1111	00
SW Dra	+69.0237	127.27	47.33	–3.22	–0.93	–30	1	–1.24	10.49	0.04	1121	00
WY Dra	+80.0305	113.08	25.14	–1.11	0.88	–6	30	–1.66	12.67	0.24	1161	00

Table 2—Continued

Star	NPM1	l	b	μ_α	μ_δ	V_{rad}	ϵ_V	[Fe/H]	$\langle V \rangle_I$	A_V	Ref	D/
		$\circ$	$\circ$	″/cent	″/cent	km/s	km/s	dex	mag	mag	[a]	[b]
XZ Dra	+64.0579	95.65	22.50	0.56	–0.71	–30	2	–0.87	10.18	0.22	1121	11
AE Dra	+55.0697	84.35	25.41	–0.83[c]	–0.24[c]	–243	30	–1.54	12.65	0.14	1161	00
BC Dra	+76.0341	107.95	28.48	–2.18	3.30	–161	26	–2.00	11.60	0.18	1161	00
BD Dra	+77.0411	108.63	28.25	–2.88[c]	0.07[c]	–253	30	–1.74	12.69	0.10	1161	00
BT Dra	+60.0453	99.41	51.21	0.13	–3.60	–156	30	–1.55	11.94	0.00	1161	00
RX Eri	–15.0672	214.26	–33.88	–1.56	–0.70	66	1	–1.30	9.68	0.08	1111	00
SV Eri	–11.0414	194.26	–53.47	1.45	–3.95	–12	9	–2.04	9.95	0.19	1111	00
XY Eri	–13.0580	207.42	–41.69	1.13	0.68	221	11	–2.08	13.02	0.08	1161	00
BB Eri	–19.0632	218.81	–34.36	3.45	0.91	235	11	–1.51	11.46	0.03	1121	00
BK Eri	–01.0185	175.80	–51.70	3.24[c]	–1.98[c]	141	10	–1.64	12.67	0.10	1161	00
SS For	–	216.42	–72.99	4.30	–7.25	–112	1	–1.35	10.10	0.00	2121	00
SW For	–	243.27	–60.75	1.25	–0.10	174	18	–1.95	12.34	0.00	2111	00
RR Gem	–	187.44	19.52	–0.35	–0.24	64	1	–0.35	11.34	0.21	2121	11
SZ Gem	+19.0314	201.85	22.08	–1.17	–3.40	307	11	–1.81	11.66	0.08	1121	00
TW Her	+30.0973	55.87	24.80	–0.32	–0.74	4	16	–0.67	11.23	0.17	1121	11
VZ Her	+36.0784	59.59	34.59	–2.44	–1.95	–115	4	–1.03	11.44	0.12	1121	00
AF Her	+41.0868	65.15	41.64	–1.62	–0.72	–268	9	–1.94	12.82	0.00	1121	00
AG Her	+40.0809	64.49	41.46	–2.15	–1.91	–103	21	–2.01	12.66	0.00	1121	00
CW Her	+35.0792	58.01	38.99	–1.65	1.31	–285	30	–2.09	12.47	0.05	1141	00
DL Her	+14.1435	36.28	26.60	1.13	–0.13	–61	14	–1.32	12.37	0.35	1141	10
GY Her	+37.1381	60.70	41.71	0.29	1.13	–157	53	–1.92	12.57	0.01	1141	00
V394 Her	+17.1675	40.01	27.39	–0.67	0.67	–74	10	–1.48	12.87	0.21	1161	00
SV Hya	–	297.08	36.59	–5.51	0.81	100	8	–1.70	10.51	0.34	2111	00
SZ Hya	–09.0958	239.77	25.93	–0.66	–3.85	140	9	–1.75	11.23	0.05	1121	00
UU Hya	+04.0500	230.41	38.18	–2.51	–1.12	295	14	–1.65	12.27	0.05	1121	00
WZ Hya	–12.1166	254.26	34.41	0.14	–1.49	304	8	–1.30	10.82	0.26	1121	00
XX Hya	–15.1036	244.59	21.35	1.86	–2.92	32	20	–1.33	11.89	0.15	1121	00
DD Hya	+02.0597	219.85	19.30	–0.70	–1.19	153	25	–1.00	12.18	0.06	1151	01
DG Hya	–05.0893	233.78	24.95	–1.08	–2.52	164	18	–1.42	12.14	0.06	1121	00
DH Hya	–09.0936	238.03	22.96	–2.37	–0.67	355	8	–1.55	12.13	0.05	1111	00
ET Hya	–08.0736	233.50	18.31	–1.66	–0.73	320	20	–1.69	12.06	0.08	1151	00
FY Hya	–	318.76	31.37	–4.12	–0.04	82	24	–2.33	12.46	0.15	2111	00
GL Hya	+02.0649	223.71	25.46	–1.34	–0.90	223	21	–1.45	12.95	0.07	1161	00
GO Hya	+06.0328	221.77	30.32	–0.23	–0.98	–25	23	–0.83	12.34	0.09	1141	11
V Ind	–	355.33	–43.12	–7.00	–9.00	202	3	–1.50	9.92	0.05	2111	00
CQ Lac	+39.0934	93.95	–14.55	0.34	–0.15	20	30	–2.04	12.43	0.45	1161	00

Table 2—Continued

Star	NPM1	l °	b °	μ_α ″/cent	μ_δ ″/cent	V_{rad} km/s	ϵ_V km/s	[Fe/H] dex	$\langle V \rangle_I$ mag	A_V mag	Ref [a]	D
RR Leo	+24.0416	208.42	53.10	–1.69	–1.26	88	1	–1.57	10.68	0.09	1111	0
RX Leo	+26.0471	209.43	70.51	0.38	–2.66	–121	6	–1.38	11.90	0.00	1111	0
SS Leo	+00.0760	265.32	57.06	–2.38	–2.79	163	3	–1.83	11.03	0.04	1111	0
ST Leo	+10.0701	253.44	66.15	–0.56	–3.37	153	4	–1.29	11.46	0.09	1121	0
SU Leo	+08.0618	228.92	43.82	0.60	–0.86	–81	30	–1.41	13.55	0.02	1161	0
SW Leo	–02.1164	255.63	48.98	–0.74	–0.68	46	11	–1.45	13.08	0.07	1161	0
SZ Leo	+08.0731	243.93	57.83	–1.60	–2.55	185	4	–1.86	12.35	0.04	1121	0
TV Leo	–05.1129	262.99	49.06	1.07	0.28	–96	5	–1.97	12.10	0.07	1111	0
WW Leo	+07.0715	226.04	38.45	–0.03	–2.63	–66	20	–1.48	12.47	0.09	1121	0
AA Leo	+10.0702	254.14	66.09	–0.26	–3.35	32	24	–1.47	12.27	0.09	1121	0
AE Leo	+17.0930	234.20	68.19	2.38	–1.25	–53	10	–1.71	12.52	0.00	1151	0
AN Leo	+06.0502	253.35	60.72	0.29	–3.06	–68	17	–1.14	12.45	0.13	1141	0
AX Leo	+12.0892	248.29	66.30	–1.85	–2.08	182	10	–2.28	12.18	0.07	1141	0
BT Leo	+18.0551	228.38	65.59	–0.90	–0.34	119	14	–0.81	13.11	0.00	1141	1
V LMi	+29.0467	201.30	57.84	2.16	–3.02	–110	7	–1.15	11.71	0.02	1121	0
X LMi	+39.0396	182.53	53.70	1.63	–2.01	–82	18	–1.68	12.31	0.00	1121	0
U Lep	–21.0669	221.10	–34.37	4.33	–5.86	128	11	–1.93	10.60	0.02	1111	0
RY Lib	–21.1628	330.87	36.08	–1.68	–0.45	33	11	–1.48	13.15	0.25	1161	0
TV Lib	–08.1548	353.16	39.67	0.05	1.04	–61	10	–0.27	11.94	0.25	1121	1
VY Lib	–15.2271	353.86	28.84	–0.22	–6.46	142	10	–1.32	11.72	0.45	1111	0
TW Lyn	+43.0251	176.15	27.54	0.69	0.86	–40	26	–1.23	11.90	0.14	1141	1
Y Lyr	+43.0988	72.67	20.87	–0.08	–0.66	–65	23	–1.03	13.28	0.18	1121	1
RR Lyr	–	74.96	12.30	–10.95	–19.42	–63	8	–1.37	7.74	0.13	2111	0
RZ Lyr	+32.1588	62.11	15.82	1.02	1.99	–233	23	–2.13	11.51	0.32	1111	0
CN Lyr	+28.1070	58.01	14.70	–0.12	–1.61	67	30	–0.26	11.49	0.62	1161	1
CX Lyr	+28.1083	58.99	12.72	–0.49	–1.30	–203	30	–1.79	12.83	0.82	1141	0
IO Lyr	+32.1543	60.59	19.98	–1.22	2.19	–157	30	–1.52	11.86	0.15	1161	0
UV Oct	–	308.40	–23.55	–6.93	–12.30	126	12	–1.61	9.42	0.21	2111	0
ST Oph	–	22.83	16.64	–0.09	–0.08	12	7	–1.30	12.05	0.60	2111	1
V413 Oph	–10.1983	4.39	25.97	–1.10	–1.62	–39	30	–1.00	12.08	0.63	1161	1
V445 Oph	–	7.91	28.45	0.47	1.24	–22	5	–0.23	10.99	0.59	2121	1
V452 Oph	+11.1284	32.52	25.72	–0.36	–0.10	–375	30	–1.72	12.18	0.41	1121	0
V964 Ori	–02.0731	202.50	–23.91	0.70	–1.21	178	11	–1.89	12.95	0.25	1151	0
TY Pav	–	330.55	–17.10	–2.10	–2.20	245	9	–2.31	12.58	0.26	2111	0
DN Pav	–	332.82	–30.80	–0.90	–3.00	–69	12	–1.54	12.42	0.14	2111	0
VV Peg	+18.1195	78.42	–30.42	–0.06	–1.22	13	8	–1.88	11.79	0.13	1111	0

Table 2—Continued

Star	NPM1	l °	b °	μ_α ″/cent	μ_δ ″/cent	V_{rad} km/s	ϵ_V km/s	[Fe/H] dex	$\langle V\rangle_I$ mag	A_V mag	Ref a	D/ b
AV Peg	+22.1796	77.44	–24.05	1.35	–1.34	–58	1	–0.14	10.44	0.14	1121	11
BH Peg	+15.1616	85.62	–38.36	–2.01	–6.71	–278	2	–1.38	10.44	0.20	1111	00
CG Peg	+24.0966	77.18	–20.75	–0.11	–0.49	–4	4	–0.48	11.11	0.20	1121	11
DZ Peg	+15.1715	93.09	–41.46	1.70	–2.49	–294	11	–1.52	12.00	0.05	1161	00
GV Peg	+26.1124	109.07	–34.83	0.69	–3.07	–335	30	–1.99	13.36	0.10	1161	00
AR Per	–	154.93	–2.27	–0.15	0.50	5	1	–0.43	10.43	1.08	2122	11
U Pic	–	257.67	–39.61	–0.10	–1.70	30	12	–0.73	11.32	0.00	2131	11
RY Psc	–02.0022	100.68	–62.89	3.99	–0.77	–1	9	–1.39	12.28	0.08	1121	00
BB Pup	–19.0790	241.28	10.27	–1.58	1.05	98	9	–0.57	12.17	0.45	1111	11
V440 Sgr	–	15.31	–19.20	–0.20	–5.00	–62	1	–1.47	10.24	0.36	2121	00
RU Scl	–	41.53	–78.86	5.63	–2.04	38	8	–1.25	10.21	0.03	2111	00
VY Ser	+01.1004	6.16	44.09	–9.84	–0.51	–145	1	–1.82	10.13	0.06	1111	00
AN Ser	+13.1114	23.80	45.24	–0.27	–1.11	–47	4	–0.04	10.97	0.09	1121	11
AR Ser	+02.1454	7.89	44.25	–3.66	0.60	132	4	–1.78	11.85	0.07	1131	00
AT Ser	+08.1225	18.03	42.45	–0.14	–1.48	–58	11	–2.05	11.45	0.08	1111	00
AV Ser	+00.1096	11.28	36.83	0.80	0.65	–45	13	–1.20	11.40	0.26	1111	10
AW Ser	+15.1229	28.67	43.35	–0.97	–1.63	–126	15	–1.67	12.79	0.04	1141	00
BH Ser	+19.0930	27.56	56.27	–0.78	–1.51	–113	11	–1.59	12.85	0.08	1161	00
CS Ser	+03.1110	7.22	45.43	2.37	–2.79	2	14	–1.57	12.39	0.08	1141	00
DF Ser	+18.0911	26.27	55.92	0.46	–0.55	–10	14	–0.74	12.69	0.07	1141	11
RV Sex	–08.0980	258.12	43.38	–0.98	–0.85	120	20	–1.10	12.30	0.02	1161	00
SS Tau	+05.0288	180.09	–38.53	0.77	0.28	–11	10	–0.28	12.50	0.49	1121	11
U Tri	+33.0093	137.89	–27.24	0.89	–1.30	6	23	–0.79	12.60	0.10	1121	11
W Tuc	–	301.66	–53.72	0.30	0.20	63	3	–1.64	11.43	0.00	2111	00
YY Tuc	–	325.32	–54.21	0.14	–0.34	56	9	–1.82	11.98	0.00	2111	00
RV UMa	+54.0419	109.75	62.06	–2.76	–4.69	–183	9	–1.19	10.78	0.01	1111	00
TU UMa	+30.0521	198.80	71.87	–7.64	–4.97	88	1	–1.44	9.81	0.00	1111	00
AB UMa	+48.0617	141.04	67.86	–1.30	–2.00	–56	26	–0.72	10.80	0.00	1141	11
ST Vir	–00.1211	346.37	53.65	–0.06	–2.65	–22	13	–0.88	11.52	0.07	1121	11
UU Vir	–	280.73	60.52	–2.96	–0.45	–8	1	–0.82	10.56	0.01	2121	11
UV Vir	+00.0808	286.55	62.28	–2.63	–1.80	99	11	–1.19	11.83	0.02	1121	00
WY Vir	–06.1416	321.78	54.28	–1.74	–1.17	181	10	–2.84	13.38	0.03	1161	00
AD Vir	–07.2115	333.18	51.21	–1.97	–0.60	134	14	–1.15	13.04	0.04	1151	00
AE Vir	+04.0956	351.61	57.27	–0.03	–1.77	208	10	–1.16	13.26	0.02	1141	00
AF Vir	+06.0757	355.48	59.16	–6.16	0.05	–35	14	–1.46	11.52	0.01	1121	00
AM Vir	–16.1465	313.94	45.52	–0.16	–5.15	99	24	–1.45	11.49	0.14	1121	00

Table 2—Continued

Star	NPM1	l °	b °	μ_α ″/cent	μ_δ ″/cent	V_{rad} km/s	ϵ_V km/s	[Fe/H] dex	$\langle V\rangle_I$ mag	A_V mag	Ref [a]	D
AS Vir	–09.1409	303.47	52.61	1.14	–3.69	70	23	–1.49	11.90	0.08	1121	0
AT Vir	–05.1349	304.66	57.40	–5.42	–1.76	346	8	–1.91	11.27	0.04	1121	0
AV Vir	+09.0882	325.01	70.82	0.64	–3.38	152	4	–1.32	11.78	0.00	1121	0
BQ Vir	–02.1373	295.38	60.23	–0.27	–1.39	129	9	–1.32	12.48	0.03	1161	0
DO Vir	–05.1546	345.60	48.45	–2.72	0.69	24	36	–0.80	14.14	0.10	1151	0
FU Vir	+13.0858	290.13	75.56	1.33	–0.77	–90	8	–1.17	12.63	0.07	1161	0
FK Vul	+22.1711	67.60	–13.92	0.05	–1.51	–76	30	–0.95	12.87	0.35	1161	1
AT And	–	109.76	–18.09	–0.20	4.60	–241	11	–0.97	10.66	0.38	2221	0
S Ara	–	343.38	–12.45	–2.34	–1.53	172	13	–1.43	10.67	0.36	2231	0
RU Boo	+23.0728	30.94	63.87	–1.35	–0.32	–60	35	–1.50	13.60	0.04	1321	0
BI Cen	–	294.66	2.44	–0.76	0.15	210	30	–0.83	11.86	0.59	2262	0
UU Cet	–17.0006	73.26	–75.09	2.68	–0.65	–114	3	–1.32	11.95	0.01	1221	0
Z Com	+18.0747	328.12	80.58	–0.77	–1.85	–50	35	–1.50	13.73	0.03	1321	0
ST Com	–	347.87	81.25	–3.61	–3.57	–68	7	–1.26	11.38	0.04	2221	0
SW Cru	–	296.49	1.91	1.07	0.19	–23	30	–0.54	12.33	1.18	2262	1
UY Cyg	–	74.54	–9.63	0.13	–0.76	–2	6	–1.03	11.05	0.22	2222	1
SW Her	+21.1016	41.68	34.00	–1.11	0.04	–130	35	–1.50	14.14	0.21	1321	0
VX Her	+18.0988	35.22	39.08	–4.70	1.66	–377	3	–1.52	10.62	0.18	1211	0
AR Her	+47.1123	74.10	48.20	–6.53	1.24	–349	8	–1.40	11.18	0.04	1211	0
RV Leo	–	232.37	51.14	–0.50	–1.30	0	35	–1.50	13.85	0.08	2321	0
TT Lyn	+44.0496	176.07	41.65	–8.41	–4.01	–67	1	–1.76	9.87	0.03	1261	0
EZ Lyr	–	65.52	16.25	–1.32	–0.20	–60	23	–1.56	11.60	0.21	2261	0
AO Peg	+18.1149	69.90	–22.60	–0.31	–2.94	115	35	–0.92	12.83	0.19	1261	0
TU Per	–	142.78	–4.29	1.51	–0.61	–377	11	–1.50	12.53	1.38	2324	0
RV Phe	–	336.01	–64.00	4.15	–1.85	–99	2	–1.60	11.75	0.06	2211	0
XX Pup	–	236.65	8.72	–3.13	–0.14	386	7	–1.50	11.20	0.38	2324	0
V675 Sgr	–	358.26	–7.83	0.00	1.20	–105	30	–2.01	10.36	0.19	2212	0
V1640 Sgr	–	0.47	–13.64	–0.40	0.90	41	10	–0.54	12.68	0.31	2251	1
V494 Sco	–	357.23	–0.49	–0.34	–0.62	26	30	–1.01	11.27	1.16	2233	1
AF Vel	–	284.16	8.60	5.90	–1.75	236	16	–1.64	11.34	0.61	2214	0
BB Vir	+06.0723	340.31	64.84	–3.71	–1.02	–38	13	–1.61	11.07	0.00	1221	0
BC Vir	+06.0660	323.42	67.52	1.55	–2.81	4	13	–1.50	12.21	0.00	1361	0
BN Vul	–	58.63	3.41	–4.85	–3.80	–267	4	–1.52	11.08	1.36	2262	0

[a]References: First digit indicates source of proper motions (1=NPM; 2=WMJ). Second digit indicates source of abundance (1=L94, Table 9; 2=ΔS from L94, Table 2 and Eqn. 6; 3=[Fe/H]=–1.5). Third digit indicates source of photometry (1=CD80; 2=Bookmyer *et al* 1977; 3=Lub 1979; 4=Schmidt *et al* 1991, 1995; 5=Layden 1996; 6=L94). Fourth digit indicates source of A_V (1=Burstein & Heiles 1982; 2=Blanco 1992; 3=FitzGerald 1968,1987; 4=interpolation).

Table 3. Disk/Halo Definitions.

Definition	Description
Disk-1	All stars lying above/rightward of $V_\theta = -400$[Fe/H]-300 (see Fig. 3).[a]
Halo-1	All stars lying below/leftward of this line.[a]
Disk-2	All stars having [Fe/H] ≥ -1.0 and $V_\theta > 80$ km s^{-1}.[b]
Halo-2	All stars excluded from Disk-2.[b]
Disk-3	All stars in Disk-1 *plus* all stars having $\lvert V_\pi \rvert < 100$ km s^{-1}, $V_\theta > 80$ km s^{-1}, $\lvert V_z \rvert < 60$ km s^{-1}, $\lvert Z \rvert < 1.0$ kpc, *and* [Fe/H] > -1.6.
Halo-3	All stars excluded from Disk-3.
Halo-1R	All stars in Halo-1 with [Fe/H] > -1.55.
Halo-1P	All stars in Halo-1 with [Fe/H] ≤ -1.55.

[a]Two stars, AO Peg and FU Vir, lie above/rightward of the line defining Disk-1, yet their extreme V_π and V_z velocities clearly indicate that they belong to the halo. They were removed from Disk-1 and included in Halo-1.

[b]AO Peg fits the definition for Disk-2, yet clearly belongs to the halo. It was removed from Disk-2 and included in Halo-2.

Table 4. Simulated Data Sets.

Data Set	Population Simulated	Space Distribution	N_{stars}	N_{trials}	Solution Set	σ_k	VE-covar included	N_{conv}
H1	halo[a]	random	165	5	H1.0	0.0	yes	5
					H1	0.1	yes	5
H2	halo[a]	real	169	5	H2.0	0.0	yes	5
					H2	0.1	yes	5
				(+15)	H2d	0.1	no	20
D1	disk[b]	random	50	20	D1	0.1	yes	19
D2	disk[b]	real	45	20	D2	0.1	yes	18
					D2d	0.1	no	18

[a]Halo $V_{(\pi,\theta,z)} = (0, 20, 0)$ km s^{-1}; $\sigma_{(\pi,\theta,z)} = (160, 100, 90)$ km s^{-1}.

[b]Disk $V_{(\pi,\theta,z)} = (0, 200, 0)$ km s^{-1}; $\sigma_{(\pi,\theta,z)} = (50, 50, 30)$ km s^{-1}.

Table 5. Monte Carlo Simulation Results.

Solution		V	σ_U	σ_V	σ_W	M_V		ΔV	$\Delta\sigma_U$	$\Delta\sigma_V$	$\Delta\sigma_W$	ΔM_V
H1.0	mean	–203	158	100	89	+0.82	mean	+3	–2	–1	–3	+0.05
	$\langle\sigma_i\rangle$	11	11	8	7	0.12	SD	5	2	7	3	0.07
H1	mean	–204	158	99	89	+0.79	mean	+2	–2	–3	–3	+0.02
	$\langle\sigma_i\rangle$	12	11	8	7	0.12	SD	5	2	6	3	0.07
H2.0	mean	–198	155	96	86	+0.84	mean	+7	–7	–3	–2	+0.07
	$\langle\sigma_i\rangle$	11	12	7	6	0.12	SD	2	5	3	4	0.08
H2	mean	–199	155	94	86	+0.82	mean	+6	–6	–4	–2	+0.05
	$\langle\sigma_i\rangle$	12	12	7	6	0.12	SD	2	5	3	3	0.08
H2d	mean	–205	155	93	87	+0.81	mean	+4	–4	–4	–2	+0.04
	$\langle\sigma_i\rangle$	12	12	7	6	0.12	SD	5	6	3	3	0.08
D1	mean	–32	51	48	29	+0.88	mean	0	–2	–1	–2	–0.02
	$\langle\sigma_i\rangle$	8	8	8	6	0.34	SD	5	7	7	7	0.44
D2	mean	–33	51	48	27	+1.04	mean	+1	–4	–4	–2	+0.13
	$\langle\sigma_i\rangle$	9	9	8	6	0.35	SD	5	6	6	5	0.29
D2d	mean	–32	51	48	26	+1.04	mean	+1	–4	–4	–3	+0.13
	$\langle\sigma_i\rangle$	9	8	8	6	0.34	SD	5	5	7	4	0.29

Table 6. Statistical Parallax Solutions.

Sample	N_{stars}	$\langle$[Fe/H]$\rangle$ dex	$\langle U \rangle$ km/s	$\langle V \rangle$ km/s	$\langle W \rangle$ km/s	σ_U km/s	σ_V km/s	σ_W km/s	M_V mag	$M_{V,corr}$ mag
Halo-1	169	–1.60	+9	–205	–11	165	102	95	+0.71	+0.71
			± 13	12	8	12	7	7	0.12	0.12
Halo-2	175	–1.58	+8	–196	–11	161	108	93	+0.72	+0.72
			± 13	12	7	12	8	7	0.12	0.12
Halo-3	162	–1.61	+9	–210	–12	168	102	97	+0.71	+0.71
			± 14	12	8	13	8	7	0.12	0.12
Halo-1R	86	–1.34	–13	–216	–13	172	92	89	+0.69	+0.69
			± 19	16	10	17	9	9	0.16	0.16
Halo-1P	83	–1.86	+31	–195	–10	154	111	100	+0.73	+0.73
			± 18	17	12	16	12	10	0.18	0.18
Disk-1	44	–0.66	+4	–34	–18	45	43	25	+1.24	+1.08
			± 8	8	6	8	8	6	0.34	0.34
Disk-2	38	–0.58	+8	–43	–19	51	47	25	+1.15	+1.01
			± 9	10	6	9	9	6	0.35	0.35
Disk-3	51	–0.76	+6	–45	–16	52	48	29	+0.94	+0.79
			± 8	9	6	8	8	5	0.30	0.30
All stars	213	–1.40	+7	–169	–14	147	115	85	+0.73	+0.73
			± 10	10	6	10	7	6	0.11	0.11

Table 7. Selected Absolute Magnitude Determinations, $M_V(RR) = a$[Fe/H]$+b$.

Reference	Method	a	b
BH86	Stat-π of 142 field RR Lyraes ($\langle$[Fe/H]$_{L94}\rangle$ = –1.32)[a]	0.	0.79 ± 0.14
SRM	Stat-π of 139 field RR Lyraes ($\langle$[Fe/H]$_{L94}\rangle$ = –1.32)[a]	0.	0.77 ± 0.14
Buonanno *et al.* 1990	GC main sequence fits to subdwarfs[b]	0.34 ± 0.14	1.1 ± 0.2
Jones *et al.* 1988	MS fit of M5 to best subdwarf ([Fe/H] = –1.4)	0.	0.86 ± 0.12
Bolte & Hogan 1995	MS fit of M92 to updated subdwarfs ([Fe/H] = –2.3)	0.	0.49
CSJ	Synthesis of several $M_V(RR)$ results	0.15 ± 0.01	1.01 ± 0.08
Jones *et al.* 1992	Baade-Wesselink of 18 field RR Lyraes (≈ CSJ)	0.16 ± 0.03	1.02 ± 0.15
Lee 1990	Synthetic HB theory, $Y_{MS} = 0.23$	0.17	0.79
Lee 1990	Synthetic HB theory, $Y_{MS} = 0.20$	0.19	0.97
Walker 1992	LMC RRs using Cepheid distance scale ([Fe/H] = –1.9)	0.	0.44 ± 0.11[c]
Gould 1995	LMC RRs using SN1987A ring distance ([Fe/H] = –1.9)	0.	$> 0.57 \pm 0.06$[c]
Ajhar *et al.* 1996	M31 cluster HBs using Cephied distance scale	0.08 ± 0.13	0.88 ± 0.21
Sandage 1990b	Sandage period shift effect	0.39	1.17 ± 0.2
Fernley 1993	Period shift using $(V–K)$ colors	0.19	0.84
Sandage 1993	Period shift with BFE T_{eff} correction	0.30	0.94

[a]Corrected to the reddening and apparent magnitude scales used in this paper, see Sec. 6.

[b]$M_V(ZAHB)$ corrected to $M_V(RR)$ using Eqn. 4 of CSJ: $V(RR) = V(ZAHB)$ – 0.05[Fe/H] – 0.20.

[c]Error estimated from details given in the cited paper.

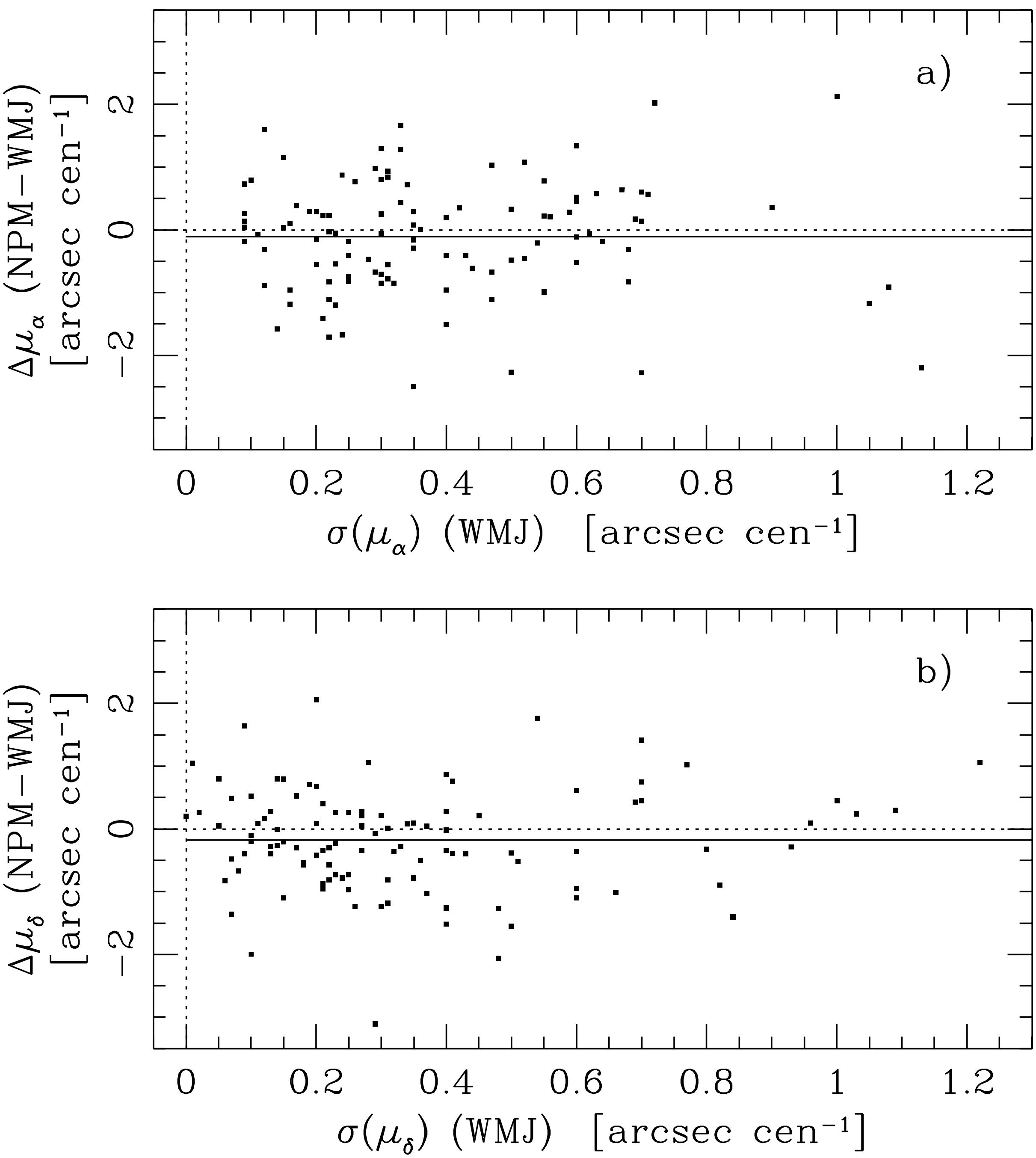

a)
b)
Δμ_α (NPM−WMJ) [arcsec cen⁻¹]
σ(μ_α) (WMJ) [arcsec cen⁻¹]
Δμ_δ (NPM−WMJ) [arcsec cen⁻¹]
σ(μ_δ) (WMJ) [arcsec cen⁻¹]

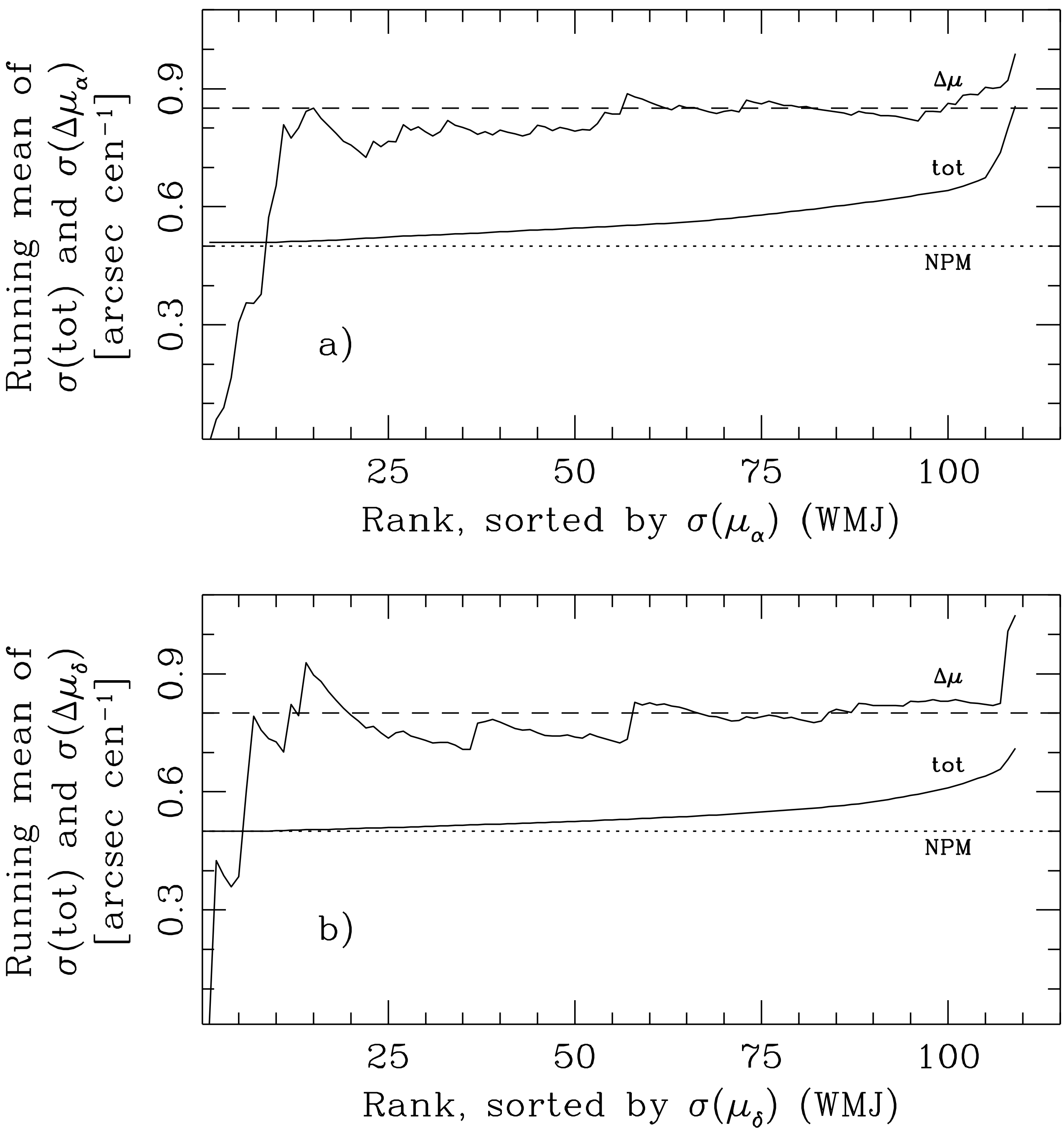

Running mean of
σ(tot) and σ(Δμ_α)
[arcsec cen⁻¹]
0.3
0.6
0.9
Δμ
tot
NPM
a)
25
50
75
100
Rank, sorted by σ(μ_α) (WMJ)
Running mean of
σ(tot) and σ(Δμ_δ)
[arcsec cen⁻¹]
0.3
0.6
0.9
Δμ
tot
NPM
b)
25
50
75
100
Rank, sorted by σ(μ_δ) (WMJ)

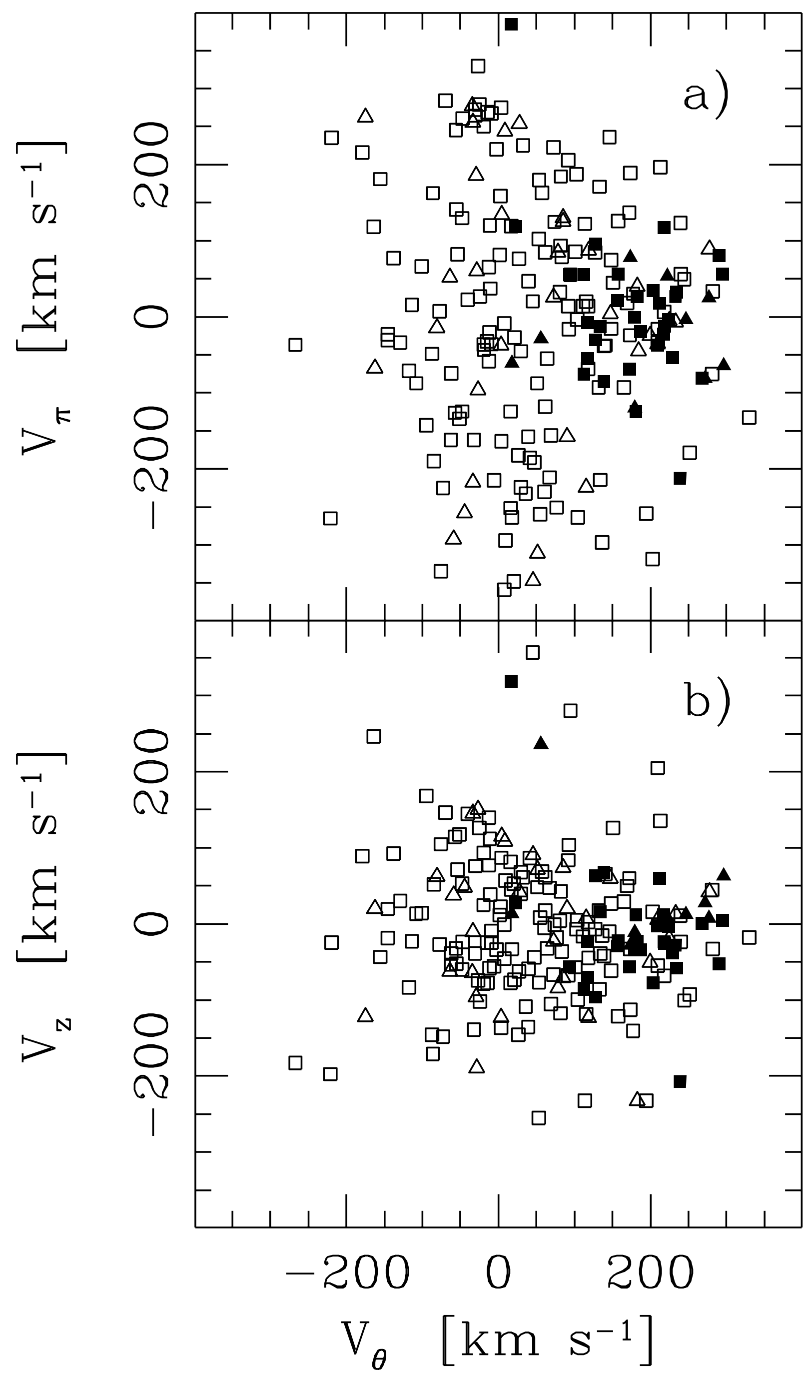

a)
b)
200
0
−200
V_π [km s^{-1}]
V_z [km s^{-1}]
−200
0
200
V_θ [km s^{-1}]

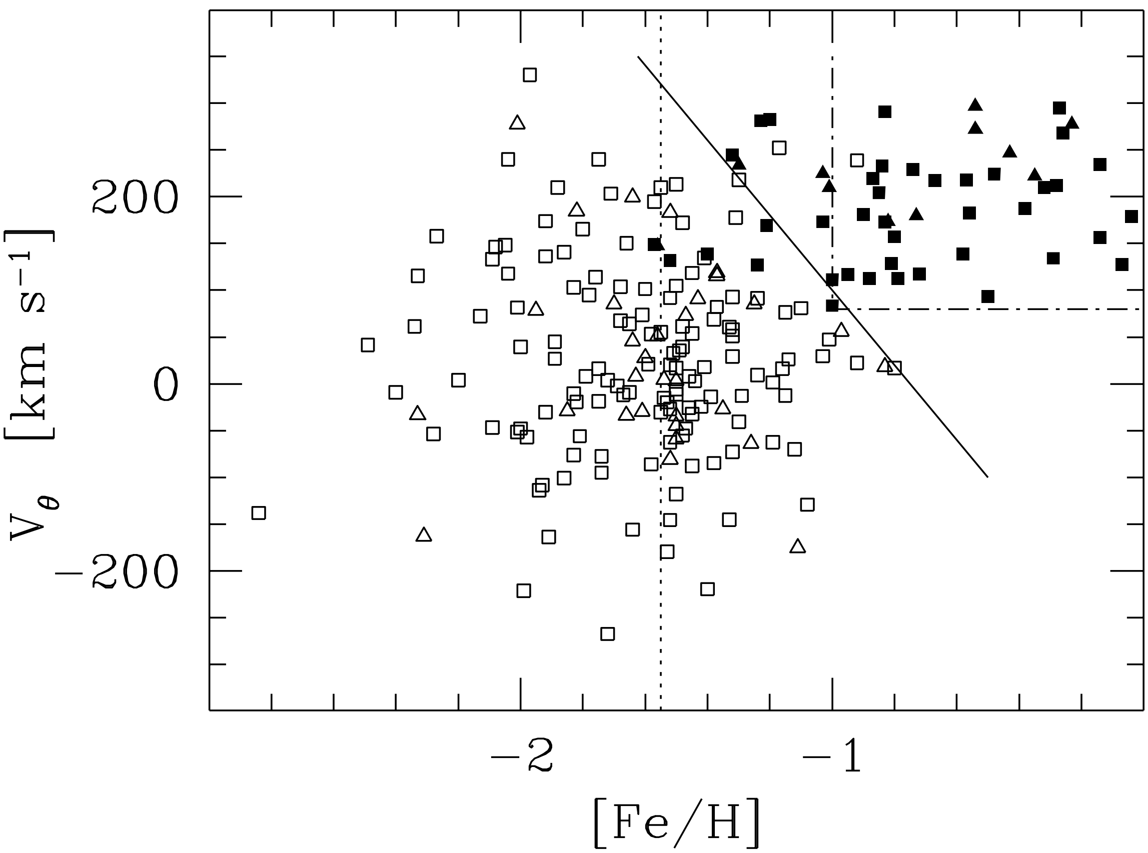

200
0
−200
V$_\theta$ [km s^{-1}]
−2
−1
[Fe/H]

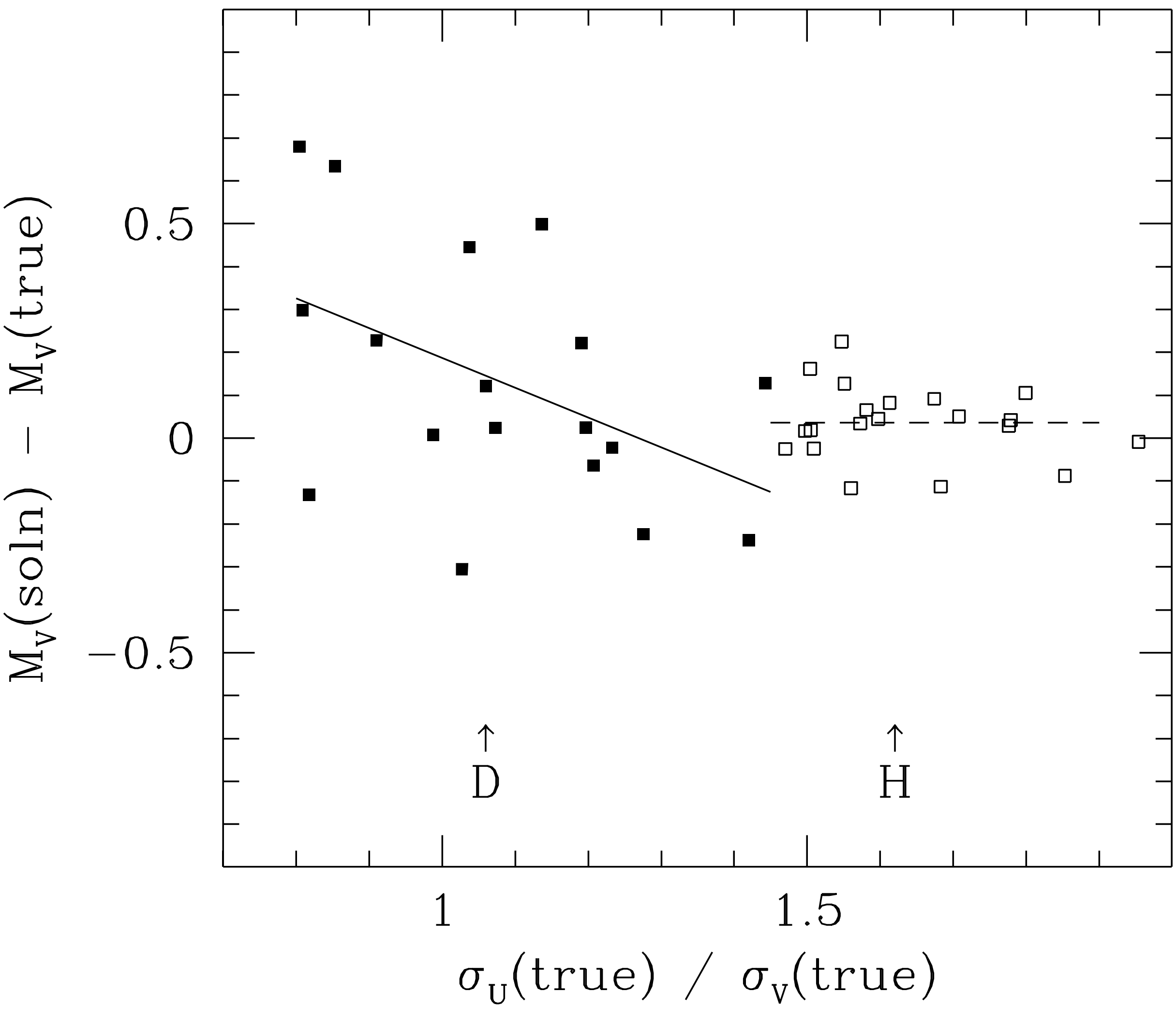

$M_V(\mathrm{soln}) - M_V(\mathrm{true})$
0.5
0
−0.5
D
H
1
1.5
$\sigma_U(\mathrm{true}) / \sigma_V(\mathrm{true})$

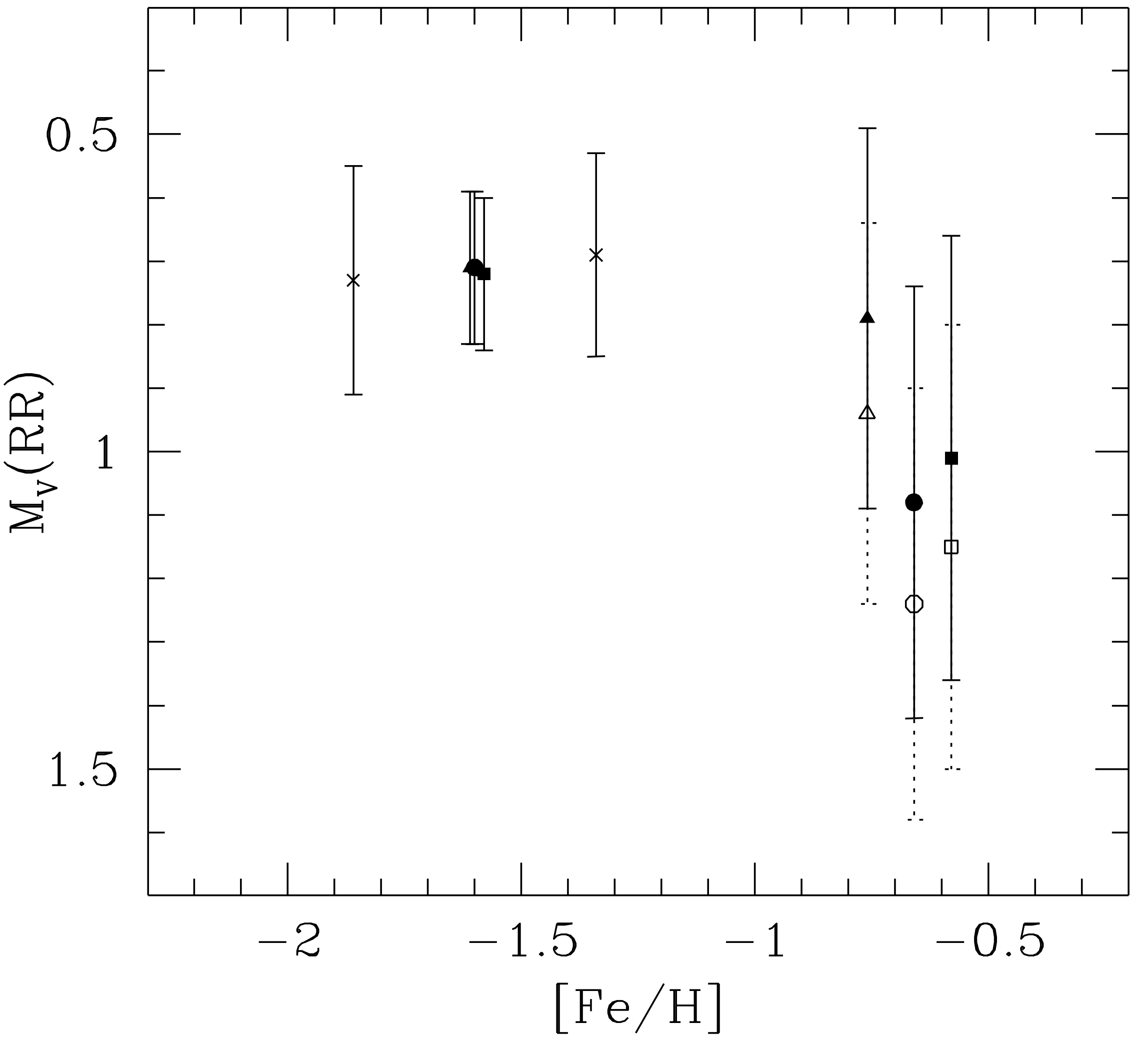
0.5
1
1.5
$M_V(RR)$
−2
−1.5
−1
−0.5
[Fe/H]

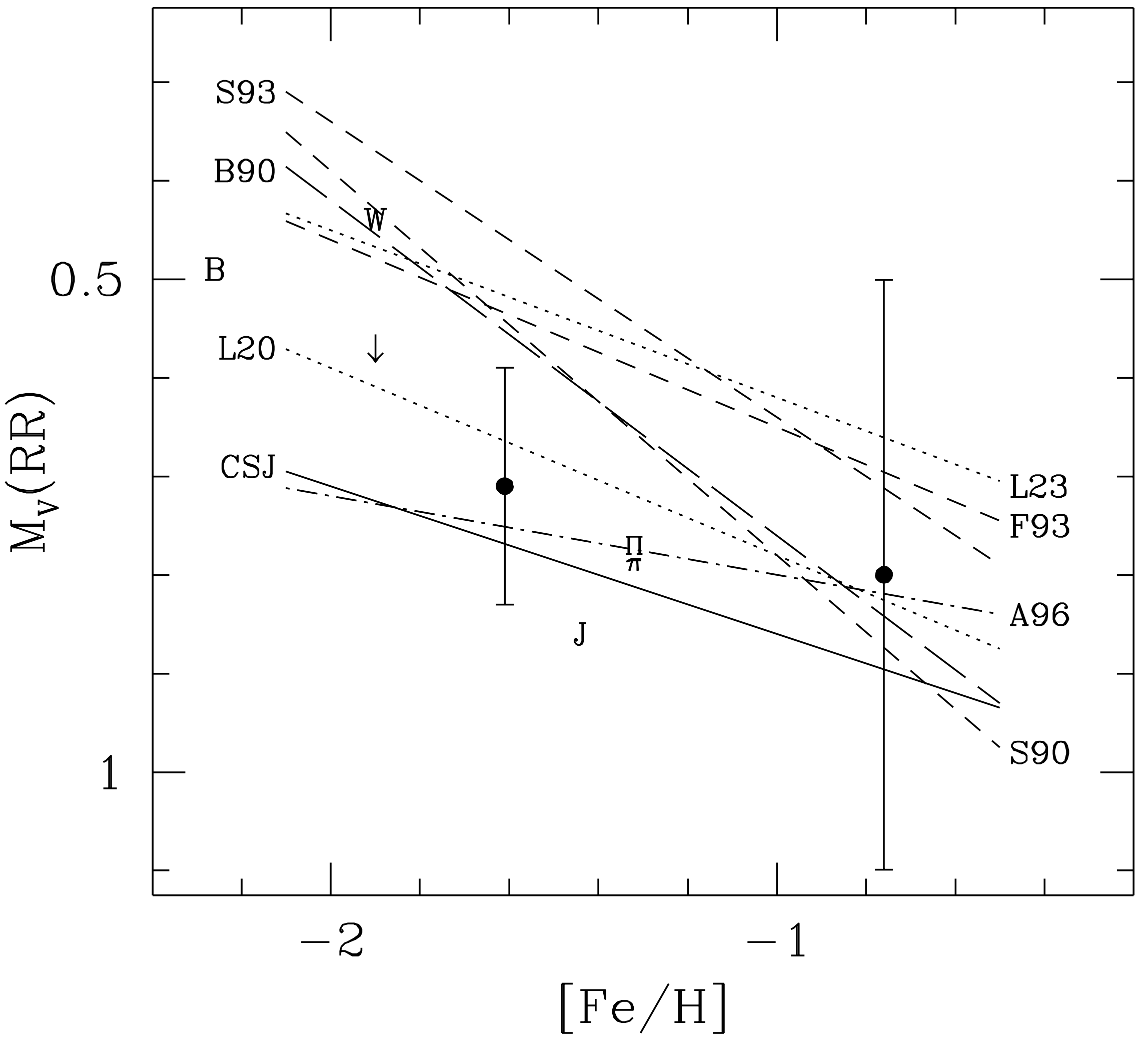

S93
B90
W
B
0.5
L20
↓
CSJ
Π
π
J
L23
F93
A96
S90
1
−2
−1
[Fe/H]
M_V(RR)

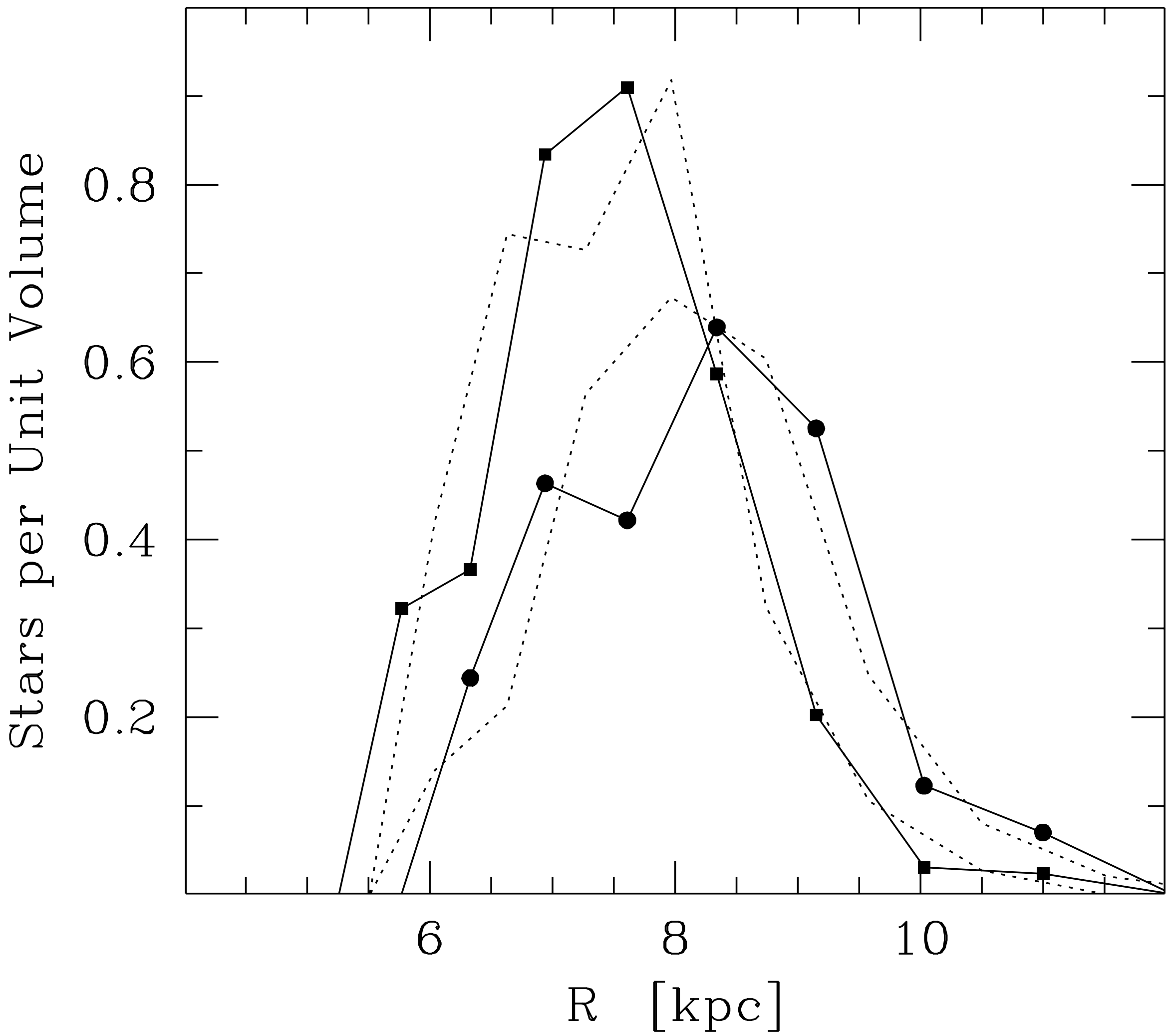
0.2
0.4
0.6
0.8
Stars per Unit Volume
6
8
10
R [kpc]